Picosecond dynamics and photoisomerization of stilbene in supersonic beams. I. Spectra and mode assignments

J. A. Syage, P. M. Felker,[a] and A. H. Zewail[b]
Arthur Amos Noyes Laboratory of Chemical Physics,[c] California Institute of Technology, Pasadena, California 91125

(Received 18 April 1984; accepted 3 July 1984)

In this and the following paper, we present a full account of our earlier report [Syage *et al.*, Chem. Phys. Lett. **88**, 268 (1982)] on the spectra and picosecond dynamics of stilbene isomerization in supersonic jets. The jet-cooled excitation and dispersed fluorescence spectra of *t*-stilbene-h_{12} and -d_{12} are reported and assigned for the $B_u \leftarrow A_g$ electronic excitation. The 0_0^0 wavelengths for h_{12} and d_{12} (in excitation) are 3101.4 and 3092.5 Å, respectively. Previously unidentified low frequency modes (as low as 20 cm^{-1} in S_0 for -h_{12}) have been observed and tentatively assigned as out-of-plane modes of a_u symmetry in C_{2h}. This indicates that *t*-stilbene has a propeller-like geometry involving phenyl rotation (i.e., C_2 symmetry). A Franck–Condon analysis of the low frequency modes and particularly the a_g, ν_{25} in-plane symmetric bend mode indicates that a large geometry change takes place upon electronic excitation possibly due to a delocalization of double bond character from the C_e–C_e bond to C_e–φ bond. The geometry change of the in-plane C_e–C_e–φ between S_1 and S_0 was determined from the Franck–Condon and a normal mode analysis to be 1.3° ± 0.3°. The rms amplitude of this bend motion for the symmetric ν_{25} bend mode (for one quanta in S_0) is $|\langle\Delta\varphi\rangle^2|^{1/2} = 1.0 \pm 0.2°$. Most a_g modes involving benzene-type vibrations (other than C–H stretch modes) have been assigned. Dispersed fluorescence spectra exhibited a broad background indicative of IVR which increased rapidly with S_1 vibrational energy. The spectra were completely diffuse above 1200 cm^{-1} which is consistent with the barrier for isomerization being at about 1100–1200 cm^{-1}. The excitation spectra show a rapid decline in intensity at higher energies due to the process of isomerization which competes with radiative decay. However, sharp (albeit weak) structure could still be discerned at energies well in excess of 2000 cm^{-1}. In the accompanying paper, we present results on the *dynamics* of isomerization and its dependence on mode mixing and the nature of the reactive surface (adiabatic vs diabatic).

I. INTRODUCTION

Picosecond laser excitation of molecules in supersonic beams has become a useful technique for direct measurements of intramolecular coherence and rates following selective vibronic excitation.[1] Recently, in a series of papers we have focused on vibrational energy redistribution and the effect of this redistribution on photochemical reactivity.[1–3] The photochemistry of isomerization has been of particular interest in this Laboratory[4–8] with major emphasis focusing on the picosecond excitation and *trans–cis* isomerization in the prototype molecule *t*-stilbene (1,2-diphenylethylene)[6–8]

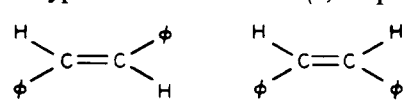

Stilbene has been studied extensively in solution.[9–11] More recently, direct time-resolved measurements of vapor phase *t*-stilbene have demonstrated that the lifetime varies with excess energy in the excited singlet state.[12] In these experiments the collision frequency of the molecules was maintained at a low enough level for the molecules to be considered collision free. The molecules in these bulb experiments, however, carried large thermal energy and therefore could not be excited into specific vibronic states to address the issue of mode specificity. In 1982, the first study of photoisomerization in a supersonic beam was reported.[6] Using the picosecond laser/supersonic jet technique[1] we were able to measure state-selective rates and to resolve vibrational modes in the S_0 and S_1 states. The measured decay rates[6] as a function of vibrational energy above the 0^0 level of S_1 showed a distinct barrier to isomerization ($\approx$3.4 kcal/mol) and allowed an assessment of the role of intramolecular vibrational redistribution (IVR) on the reaction rates. Furthermore, previously unknown low frequency modes in the isolated molecule were observed. Excitation and absorption spectra of jet-cooled *t*-stilbene by Amirav and Jortner[13] and Zwier *et al.*[14] provided relative quantum yields which showed consistency with the barrier being $\approx$3.4 kcal/mol. Finally to learn more about the effect of intermode coupling and the potential energy surface, we have recently extended our interest in isomerization to other related molecules, having reported on styrene[4] and diphenylbutadiene.[5]

The work presented here represents a full account of our earlier report on stilbene.[6] In this and the following paper, we will be addressing: (i) the spectroscopy of jet-cooled *t*-stilbene-h_{12} and -d_{12}; and (ii) selective picosecond excitation and the time-resolved dynamics of isomerization. In coming papers, we will present studies on the direct measurement of

[a] IBM Predoctoral Fellow.
[b] Camille and Henry Dreyfus Foundation Teacher–Scholar.
[c] Contribution No. 7013.

 0021-9606/84/234685-21$02.10 © 1984 American Institute of Physics

Downloaded 21 Dec 2005 to 131.215.225.171. Redistribution subject to AIP license or copyright, see http://jcp.aip.org/jcp/copyright.jsp

IVR and coherence effects (i.e., as quantum beats). The intent of this work is to shed light on interactions critical to isomerization.

Here in paper I, we report on the vibrational assignments of the S_0 and S_1 electronic states. In previous spectroscopic studies of *t*-stilbene,[15–19] the molecule was prepared in crystals (or powders), mixed crystals, and glasses where lattice interactions perturb the vibrational frequencies and Franck–Condon factors. Furthermore, the important low frequency torsional modes, which are crucial to isomerization, could be very sensitive to the matrix or solvent environment. Thermal vapor phase studies (i.e., bulbs) lead to spectral congestion. Because of the supersonic expansion, the excitation and dispersed fluorescence spectra presented here and before[6,13,14] are free of the problems associated with solids or bulbs. In the present account, we specifically examine in detail: (1) manifestations of mode couplings (e.g., Fermi resonances, vibronic interactions); (2) low frequency modes and their involvement along the reactive surface for isomerization; and (3) geometry changes which occur upon excitation as determined by relaxed symmetry restrictions, changes in vibrational frequencies and Franck–Condon analysis.

II. EXPERIMENTAL

The *t*-stilbene-h_{12} (Aldrich 96%) was recrystallized in ethanol to give 99 + % purity as determined by gc. The *t*-stilbene-d_{12} (Merck, 98% d atom) was used as is. Two sets of supersonic beam apparatus were used to record the spectra in this paper and are described in detail elsewhere.[2,3] Excitation spectra were recorded using a pulsed jet system[3] and the dispersed fluorescence spectra using both the pulsed system and a continuous jet system.[2] We give a brief description below.

A. Pulsed jet apparatus

The pulsed jet relies on a low inductance solenoid modified to deliver pulse widths of typically 250 μs when driven by a pulsed amplifier (10 kW peak power). A digital temperature controller is used to maintain the nozzle temperature to better than 1 °C. A YAG pumped dye laser (5 ns pulses) was operated at 15 Hz. UV pulses were generated with a KDP crystal whose angle was optimized via a computer controlled feedback system, thus allowing continuous UV scans.

t-Stilbene-h_{12} or -d_{12} was heated to 80–90 °C and expanded through a 300 μm aperture with a backing pressure of 50 psi He (we also used Ne and N_2). The nozzle-to-laser distance was 1.5–2.0 cm, where cooling was determined to be complete as indicated by constant rotational bandwidths and hot band intensities at longer distances. Our compact beam is pumped by a 4 in. diffusion pump which maintained an ambient pressure in the expansion chamber of less than 5×10^{-4} Torr.

The excitation spectra were recorded by collecting the fluorescence via $f/1$ optics and using a Schott WG345 cutoff filter and a Corning 7-60 bandpass filter to eliminate scattered laser light. Dispersed fluorescence spectra were recorded using a Jarrell Ash 0.5 m monochromator with slit resolution of 1 Å. UV fluorescence was detected by an EMI6256B PMT. The fluorescence signal was normalized with respect to laser intensity using a 1P28 PMT, which detected a small portion of the UV laser output. The PMT outputs were fed into a dual channel boxcar integrator (requiring a preamp for dispersed fluorescence signals). The normalized output was then digitized by a voltage to frequency converter and stored on floppy disk.

B. Continuous jet apparatus

The continuous jet apparatus is equipped with a 12 in. ring jet diffusion pump capable of maintaining 10^{-4} Torr ambient pressure during normal operation. The jet is excited with a picosecond dye laser, synchronously pumped by a mode-locked argon ion laser. The dye pulses were cavity dumped (variable from 0.8 to 4 MHz) and frequency doubled with $LiIO_3$ to give UV pulses with temporal and frequency pulse widths (FWHM) of $\approx$15 ps and $\approx$0.3 Å, respectively.

The *trans*-stilbenes were heated to $\approx$100 °C and expanded through a 150 μm pinhole. All expansions in the continuous jet were backed by 35 psi of either He or Ne unless otherwise noted. Excitation of the jet cooled molecules occurred 4–5 mm from the nozzle where it was determined that collision-free conditions had been attained. The fluorescence was collected using $f/1$ optics and imaged onto the slit of a microprocessor-controlled 0.5 m monochromator and detected by a photon counting PMT. Data were collected on a multichannel analyzer and transferred to a PDP 11/23.

C. Wavelength calibration

The dye laser and monochromator wavelength scales were calibrated against known Ne lines observed in a Fe–Ne discharge lamp (see Refs. 2 and 3 for further details). The vibrational intervals observed in the excitation spectra are reported to an accuracy of 0.5 cm^{-1} or 0.1%, whichever is larger. Assignments from the dispersed fluorescence spectra are reported to an accuracy of 3–5 cm^{-1}. Vacuum corrections have been made. The relative intensities in the resolved fluorescence spectra have not been corrected for the spectral response of the PMT.

III. RESULTS

A. Preliminaries: Molecular symmetry notation and vibronic properties

We adopt the symmetry designations for C_{2h} to describe *t*-stilbene. This would correspond to a geometry in which the phenyl groups are in-plane with the ethylene bond. The out-of-plane symmetry axis is defined as the *z* axis and hence, the S_1 state is designated as ^1B_u. The transition dipole moment lies along the long (in-plane) axis of *t*-stilbene and corresponds to the $^1B_u(\pi\pi^*) \leftarrow {}^1A_g$ transition.[15,20] The vibrationless electronic transition (i.e., 0_0^0) was detected at 3101.4 Å (h_{12}) and 3092.5 Å (d_{12}). When adjusted to vacuum, this corresponds to frequencies of 32 234.2 cm^{-1} (h_{12}) and 32 327.5 cm^{-1} (d_{12}) which we report to an accuracy of 2 cm^{-1}.

For strict C_{2h} symmetry and in the absence of vibronic

Downloaded 21 Dec 2005 to 131.215.225.171. Redistribution subject to AIP license or copyright, see http://jcp.aip.org/jcp/copyright.jsp

coupling to near lying electronic states, only a_g vibrations are active in absorption and emission from the vibrationless (a_g) levels. A reduction in molecular symmetry can arise from the out-of-plane rotation of the phenyl groups and induce activity for b_g (C_i) or a_u (C_2) modes. The ordering of mode numbers according to C_{2h} symmetry elements for *t*-stilbene (and other diphenylpolyenes[21]) has varied in the past.[16,21–23] Spectral evidence in this paper suggests that *t*-stilbene most closely resembles C_2 geometry. Hence, in order to group the modes under this reduced symmetry, we choose to order the modes in C_{2h} as a_g (ν_1 to ν_{25}), a_u (ν_{26} to ν_{37}), b_g (ν_{38} to ν_{48}), and b_u (ν_{49} to ν_{72}). When appropriate, the *t*-stilbene modes are also associated with benzene type modes (and denoted by brackets [ ]) using Varsanyi's numbering scheme for substituted benzenes.[24] We refer to vibronic transitions as A_n^m, where A is the mode number and n and m are the number of quanta of mode A in the ground and excited electronic state, respectively. Combination bands are consequently expressed as $A_n^m B_{n'}^{m'} \cdots$ and excited state SVL's as $A^m B^{m'} \cdots$.

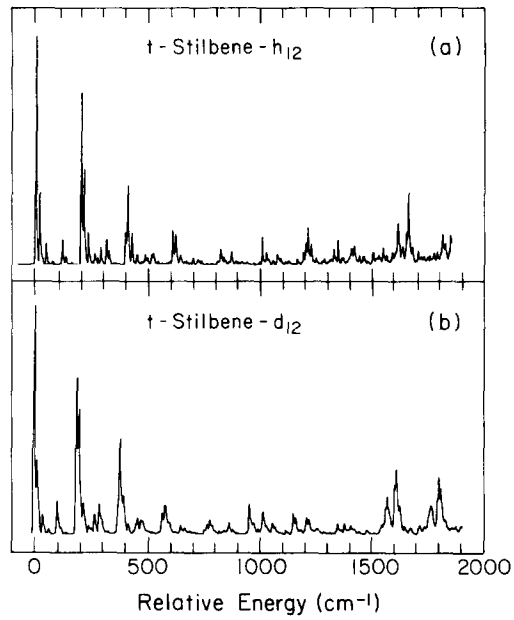

FIG. 1. Dispersed fluorescence spectra of (a) *t*-stilbene-h_{12} and (b) *t*-stilbene-d_{12} recorded for 0_0^0 excitation. Expansion conditions were 35 psi He and 100 °C sample temperature. All other conditions are given in the experimental.

B. Assignment of ground state vibrations

The ground state vibrations are analyzed from dispersed fluorescence spectra of *t*-stilbene-h_{12} and -d_{12} resulting from 0_0^0 excitation. The assignments are based primarily on comparison with IR and Raman studies of *t*-stilbene and its deuterated counterparts[16–18] as well as from comparison with spectra of other substituted benzenes,[25] particularly styrene.[4,26] Although most of the ground state modes of *t*-stilbene are known to a high degree of accuracy, the analysis of the vibronic transitions in the jet-cooled dispersed fluorescence spectra presented here is important for a number of reasons, e.g.: (i) very low frequency torsional modes are revealed for the first time; (ii) a detailed analysis of combination bands is presented; (iii) the observed vibronic intensities for known S_0 vibrational modes aid in the assignment of the S_1 modes (Sec. III C); (iv) the vibronic transitions must be identified in order to understand the dispersed fluorescence spectra resulting from higher SVL excitation; and (v) differences in the mode frequencies between vapor phase and solid phase *t*-stilbene can be interpreted in terms of geometry differences and lattice forces.

The 0^0 level dispersed fluorescence spectra of *t*-stilbene-h_{12} and -d_{12} appear in Fig. 1 and the assignments of all prominent lines in Table I. The observed fundamentals of a_g symmetry, are tabulated in Table III and compared to IR and Raman work on powders[16] and calculations.[22] The jet-cooled spectroscopy of *t*-stilbene is compared with a recent work on styrene[4] with regard to mode frequencies and vibronic intensities in Table IV. We will be referring to Tables III and IV extensively in the following discussion.

1. Ethylene and low frequency modes in S_0

In Fig. 2, the high resolution 0^0 level fluorescence spectra of the low energy region of both -h_{12} and -d_{12} compounds are shown. The most prominent mode in both dispersed fluorescence and excitation spectra is the symmetric in-plane ethylene bend ν_{25} which is observed in the ground state at 204 cm^{-1} (h_{12}) and 191 cm^{-1} (d_{12}). In Fig. 2, a long progression is evident for this mode with overtones 25_n^0 observable to $n = 4$ quanta. The overtones appear to be very harmonic on the basis of the frequency spacings. The very low frequency vibrations which build on the 25_n^0 progression will be discussed shortly.

The ν_{25} ethylene mode is observed to form strong combinations with most other vibrations including benzene type modes (Table I). Other features which deserve comment (which we mention for the -h_{12} compound) are the modes at 404, 624, and 646 cm^{-1} which lie very near to the overtones $25_2^0 = 413$ and $25_3^0 = 612$ cm^{-1}. The position of the 25_2^0 band appears to be displaced from the harmonic frequency of 408 cm^{-1}, but this may possibly be due to Fermi resonance with the 404 cm^{-1} mode. The benzene type modes which lie just to the blue of the 25_3^0 overtone appear remarkably similar to the low frequency modes which build on the 0_0^0 (Fig. 2), however, the identification as benzene type modes has been ascertained (Sec. III B 2) from SVL spectra (e.g., Fig. 3) and the frequencies found to be in excellent agreement with Raman/IR work[16] (Table III). The same behavior for the 25_n^0 progression and near lying bands is observed in *t*-stilbene-d_{12}.

Several low frequency bands in Figs. 1 and 2 were reported for the first time in our earlier work.[6] The most intriguing are the bands at 20 and 44 which may be part of a progression. That the mode interval increases with quantum number is unusual, though not implausible for torsional motions. This property is exhibited by flat bottomed potentials which reflect unrestricted large amplitude motion.[27] A similar pattern for separation of overtones was also observed for the 38 cm^{-1} C_e–φ torsion in styrene.[27] A possible assignment of the 20 cm^{-1} mode is the C_e–φ torsion of a_u symmetry, ν_{37}, which calculations indicate occurs at 38 cm^{-1} and

Downloaded 21 Dec 2005 to 131.215.225.171. Redistribution subject to AIP license or copyright, see http://jcp.aip.org/jcp/copyright.jsp

Table I. Assignment of the 0^0 level Dispersed Fluorescence Spectrum of trans-Stilbene.

t-Stilbene-h_{12}			t-Stilbene-d_{12}		
Frequency[a] (cm^{-1})	Relative Intensity[b]	Assignment[c,d]	Frequency[a] (cm^{-1})	Relative Intensity[b]	Assignment[c,d]
0.0	100	0_0^0	0.0	100	0_0^0
20	28	37_1^0 (a_u) ?	17	22	37_1^0 (a_u) ?
44	8.4		40	8.0	
75	3.0	37_1^0 (a_u) ?	67	3.9	37_1^0 (a_u) ?
119	12	36_1^0 (a_u) ?	105	13.6	36_1^0 (a_u) ?
135	3.2	$(20)_1^0(119)_1^0$	121	3.8	$(105)_1^0(17)_1^0$
159	1.1	$(44)_1^0(119)_1^0$	191	70	25_1^0
204	71	25_1^0	204	42	$25_1^0(17)_1^0$
218	39	$25_1^0(20)_1^0$	222	12	$25_1^0(40)_1^0$
235	13	$25_1^0(44)_1^0$, 116_2^0 ?	231	sh	35_1^0 (a_u) ?
264	3.7	35_1^0 (a_u) ?	245	2.5	
277	2.6		258	2.2	
290	5.8	$24_1^0[9b]_1^0$	272	5.6	$24_1^0[9b]_1^0$
318	12	$25_1^0(119)_1^0$	291	8.5	$25_1^0(105)_1^0$
328	5.3	$25_1^0(119)_1^0(20)_1^0$	382	7.6	25_2^0 Fermi Resonance ?
353	1.4	$25_1^0(119)_1^0(44)_1^0$	388	38	
404	13	25_2^0 Fermi Resonance ?	403	12	$25_2^0(17)_1^0$
413	28		423	2.2	$25_2^0(40)_1^0$
433	13	$25_2^0(20)_1^0$	467	9.6	$24_1^025_1^0$?
456	4.6	$25_2^0(44)_1^0$	483	8.3	$25_2^0(105)_1^0$
491	4.4	$24_1^025_1^0$	576	9.2	25_3^0
501	2.8	$24_1^025_1^0(20)_1^0$	592	14	$23_1^0[6b]_1^0$
528	5.0	$25_1^0(119)_1^0$	610	1.8	$22_1^0[6a]_1^0$
612	14	25_3^0	656	2.7	$25_2^024_1^0$?
624	11	$23_1^0[6b]_1^0$	676	2.7	$25_2^024_1^0(17)_1^0$
646	3.5	$22_1^0[6a]_1^0$	696	2.1	
700	2.6		760	2.4	
723	2.3	$25_3^0(119)_1^0$	775	1.9	$25_2^024_1^0(17)_1^0(105)_1^0$
738	2.0		786	5.4	$19_1^0[18a]_1^0$
822	5.9	25_4^0 or $23_1^025_1^0$	828	2.2	$18_1^0[18b]_1^0$?
838	2.8	$25_4^0(20)_1^0$	847	2.7	$21_1^0[1]_1^0$?
870	5.7	$21_1^0[1]_1^0$	872	4.0	$16_1^0[9a]_1^0$
889	1.9		887	2.9	
1006	11	$20_1^0[12]_1^0$	962	16	$20_1^0[12]_1^0$
1026	4.6	$19_1^0[18a]_1^0$	980	3.7	25_5^0 ?
1055	1.8		1001	3.7	
1072	3.8	$18_1^0[18b]_1^0$	1023	11	13_1^0
1087	2.4		1063	4.7	$16_1^025_1^0$
1123	2.1		1126	2.7	$14_1^0(105)_1^0$
1162	2.3	$17_1^0[15]_1^0$?	1152	12	$15_1^0[13]_1^0$
1188	4.2	$16_1^0[9a]_1^0$	1164	7.2	$15_1^0(17)_1^0$
1208	13	$15_1^0[13]_1^0$	1181	2.6	$15_1^0(40)_1^0$
1221	6.1	$15_1^0(20)_1^0$	1212	8.2	$14_1^025_1^0$
1245	2.3	$15_1^0(44)_1^0$	1224	6.4	$14_1^025_1^0(17)_1^0$
1281	2.0		1258	2.5	$15_1^0(105)_1^0$, $16_1^025_2^0$
1321	5.1	13_1^0	1351	3.8	$15_1^025_1^0$?
1340	6.8	$12_1^0[14]_1^0$	1367	2.4	$10_1^0[19a]_1^0$?
1359	4.2	$12_1^0(20)_1^0$?	1380	4.3	

Downloaded 21 Dec 2005 to 131.215.225.171. Redistribution subject to AIP license or copyright, see http://jcp.aip.org/jcp/copyright.jsp

TABLE I (*continued*).

1396	3.5	$16_1^0 25_1^0$
1413	5.6	$15_1^0 25_1^0$
1435	3.8	
1452	3.0	$(1435)_1^0(20)$
1475	2.1	$(1435)_1^0(44)_1^0$
1495	2.8	10_1^0 [19a]$_1^0$?
1541	4.3	$12_1^0 25_1^0$
1584	2.3	9_1^0 [8b]$_1^0$?
1607	13	8_1^0 [8a]$_1^0$
1628	4.6	$8_1^0(20)_1^0$
1654	20	7_1^0
1673	3.3	$7_1^0(20)_1^0$
1698	2.3	$7_1^0(44)_1^0$
1766	1.8	$7_1^0(119)_1^0$
1807	8.1	$8_1^0 25_1^0$
1822	5.5	$8_1^0 25_1^0(20)_1^0$
1855	13	$7_1^0 25_1^0$
2014	3.7	$8_1^0 25_2^0$
2034	3.6	$8_1^0 25_2^0(20)_1^0$
2052	5.5	$7_1^0 25_2^0$
2063	5.4	
2256	1.5	$7_1^0 25_3^0$
1399	3.4	
1411	3.2	$15_1^0 24_1^0$
1482	2.7	$14_1^0 24_1^0$?
1549	5.1	9_1^0 [8b]$_1^0$?
1573	14	8_1^0 [8a]$_1^0$
1613	30	7_1^0
1628	13	$7_1^0(17)_1^0$
1651	4.6	$7_1^0(40)_1^0$
1677	3.7	
1719	3.6	$7_1^0(105)_1^0$
1741	3.2	
1769	9.5	$8_1^0 25_1^0$
1805	28	$7_1^0 25_1^0$
1818	14	$7_1^0 25_1^0(17)_1^0$
1836	6	$7_1^0 25_1^0(40)_1^0$?
1882	4	
1935	4.7	20_2^0
1963	4.2	$8_1^0 25_2^0$
2000	14	$7_1^0 25_2^0$

[a] Frequencies are reported relative to the 0_0^0 to an accuracy of 5 cm^{-1}; [b] sh denotes shoulder; [c] Notations in brackets [ ] designate benzene-like modes using Varsanyi's (Ref. 24) numbering convention; [d] Indented assignments denote fundamentals. Modes of uncertain assignment that appear in combinations are enclosed in parentheses ( ) with their frequency.

has significant vibronic intensity for C_2 molecular symmetry.[22]

Other low frequency bands were observed in the 0^0 level fluorescence spectra at 75 and 119 cm^{-1} ($-h_{12}$). We tentatively associate these bands with the 83 and 95 cm^{-1} bands observed in S_1. The symmetry is not certain, however, evidence presented later (Secs. III C 1 and IV B 2) suggests that they are most probably a_u. Further support for this symmetry assignment is found in calculations[22] which predict that only a_u modes exist below 80 cm^{-1}. It should be mentioned that bands near to 119 cm^{-1} have been observed before[15,16] and assigned as a C_e–φ torsion of b_g symmetry[16,22] which has a calculated frequency[22] of 121 cm^{-1}. Another study[17(a)] assigns this band to an overtone of a b_g torsion. We cannot rule out either of these assignments, but feel that the presence of the a_u 20 cm^{-1} band favors an a_u symmetry for the 119 cm^{-1} mode as well.

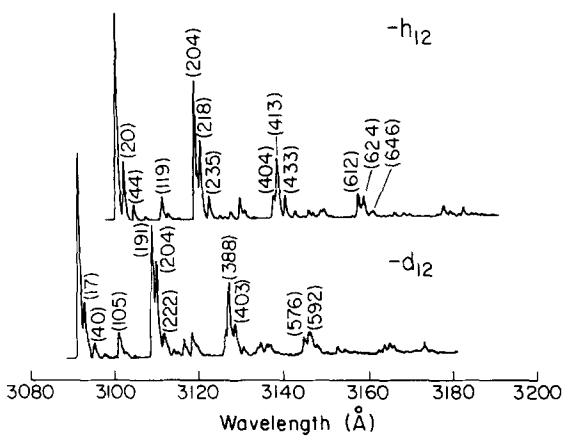

FIG. 2. Expanded view of the low energy region of the 0^0 level dispersed fluorescence spectra of the *t*-stilbenes. Numbers in parentheses denote the frequency shift from the 0_0^0.

The 7_1^0 transition, corresponding to the ethylene stretch, is strong in emission and occurs at mode frequencies of 1654 cm^{-1} (h_{12}) and 1607 cm^{-1} (d_{12}). The values are slightly larger, but in good agreement with the powder spectra[16] (Table III). Likewise, a strong correlation with styrene is observed with regard to frequency and vibronic intensity (Table IV).

2. Benzene-type modes in S_0

The assignments of the benzene-type modes rely heavily on Raman and IR spectra of powders,[16–18] the deuterium shifts, comparison of frequencies and vibronic intensities with styrene,[4] and calculations.[22] Probably, the strongest argument in favor of a mode assignment, however, is the appearance of a strong $A\,1_1^1$ emission band following $A\,1_0^1$ excitation of a suspected fundamental. This observation also leads to the identification of excited electronic state modes as well

Downloaded 21 Dec 2005 to 131.215.225.171. Redistribution subject to AIP license or copyright, see http://jcp.aip.org/jcp/copyright.jsp

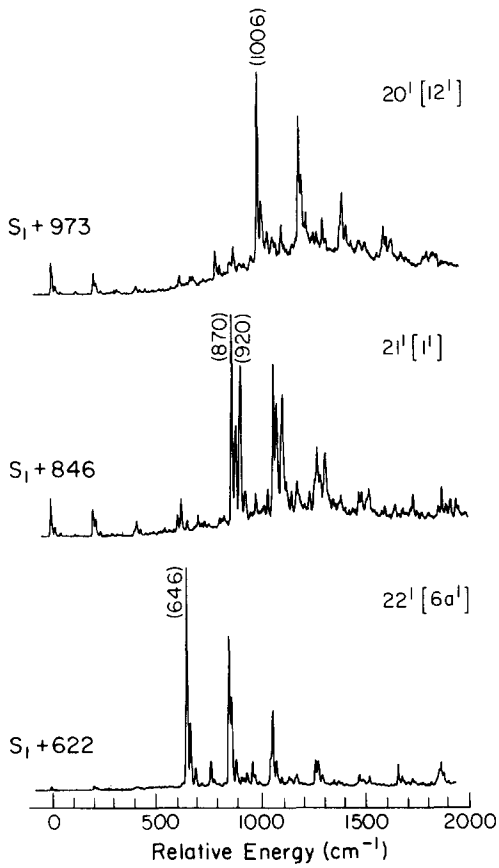

FIG. 3. Dispersed fluorescence spectra of *t*-stilbene-h_{12} following SVL excitation to benzene type modes in S_1. The false origins represent the A_0^1 emission following A_0^1 excitation. Hence, the value of the frequency displaced from the excitation frequency (denoted in parentheses) represents an interval in S_0.

(Sec. III C). Even so, many fundamentals cannot be positively assigned on account of the generally weak vibronic intensities observed for many of the benzene-type modes. A similar situation was encountered in the jet-cooled spectra of styrene.[4] We discuss the S_0 modes beginning with the assignments of greatest certainty. Tables III and IV summarize the results of the analysis.

Modes ν_{16} to ν_{23} ($[\nu_{9a}]$,$[\nu_{15}]$,$[\nu_{18b}]$,$[\nu_{18a}]$,$[\nu_{12}]$, $[\nu_1]$,$[\nu_{6a}]$,$[\nu_{6b}]$): The assignments of these vibrations (Table III) are based on the method described above of recording SVL dispersed fluorescence spectra corresponding to the excitation of these modes in S_1. We illustrate representative spectra in Fig. 3. Good agreement with the IR/Raman work[16] for both *t*-stilbene-h_{12} and -d_{12} was observed (Table III) which lends further support to the assignments. Likewise, the general similarity of the frequencies and vibronic intensities with styrene (Table IV) is supportive.

Modes $\nu_8[\nu_{8a}]$,ν_{13},$\nu_{15}[\nu_{13}]$,$\nu_{24}[\nu_{9b}]$: SVL fluorescence spectra were not very useful in assigning ν_8, ν_{14}, and ν_{15} since the fluorescence was diffuse at these higher excitation energies. The low frequency mode ν_{24} was also difficult to assign from SVL spectra since the corresponding mode in S_1 is overlapped with a strong combination band. Nonetheless, the good correspondence with the IR/Raman work[16] (Table III) and the styrene spectroscopy[4] (Table IV) argues favorably for the assignments reported.

The remaining benzene-type modes that are assigned in Tables III and IV are very tentative and are indicated as such. They represent the best guess in view of the available information. A primary consideration in associating these transitions to fundamentals was the inability to associate the observed frequencies with any likely combination bands. The intensities of these assigned fundamentals, however, are in good agreement with calculated vibronic intensities.[22]

C. Assignment of the excited state vibrations

The S_1 vibrations are analyzed from fluorescence excitation spectra which are illustrated for *t*-stilbene-h_{12} and -d_{12} in Figs. 4 and 5. An expanded intensity scale is used to reveal the very weak transitions observed at higher energies. The sharp decline in intensity at higher vibrational energies is due to the decrease in the fluorescence quantum yield resulting from isomerization. (We discuss the time-resolved dynamics of isomerization in the following paper.)

Although high resolution vapor phase spectra of *t*-stilbene-h_{12} have been presented recently,[13,14] no vibrational assignments were reported. An earlier study[15] on the absorption of *t*-stilbene in crystals and mixed crystals identifies some fundamentals, but is not of sufficient resolution to offer an extensive vibrational analysis. The analysis of the jet-cooled spectra of *t*-stilbene-h_{12} and -d_{12} reported here rely on: (i) comparison with calculations; (ii) comparison with the analyzed jet-cooled spectra of styrene; (iii) deuterium effects; and (iv) comparison with ground state assignments and vibronic intensities discussed in the previous section. We use the technique described earlier of analyzing dispersed flu-

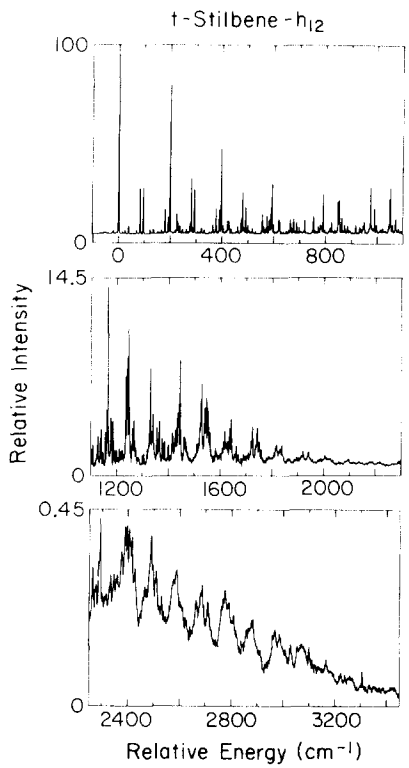

FIG. 4. Fluorescence excitation spectra of *t*-stilbene-h_{12} for the $^1B_u \leftarrow {}^1A_g$ electronic transition. Spectra were recorded under expansion conditions of 50 psi He and 80 °C sample temperature. All other conditions are given in the experimental.

Downloaded 21 Dec 2005 to 131.215.225.171. Redistribution subject to AIP license or copyright, see http://jcp.aip.org/jcp/copyright.jsp

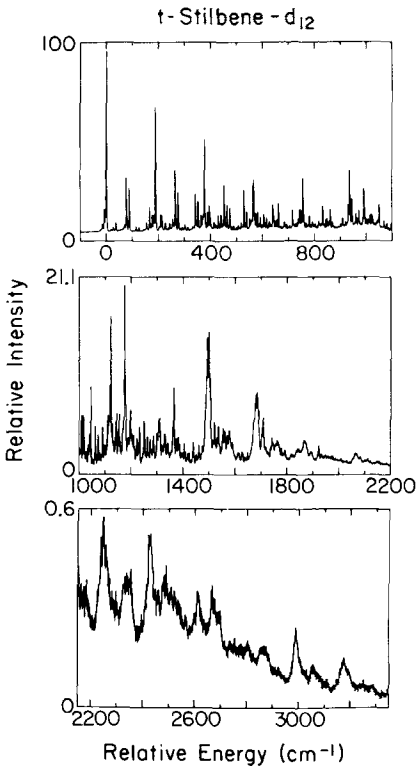

FIG. 5. Fluorescence excitation spectra of *t*-stilbene-d_{12} for the $^1B_u \leftarrow {}^1A_g$ electronic transition. Expansion conditions were 50 psi He and 80 °C.

orescence spectra obtained by exciting specific lines in the excitation spectra. Again we mention that if mode A is excited in S_1 (i.e., A_0^1), then according to Franck–Condon considerations, the transition A_1^1 should be strong in emission and possibly appear as a false origin in the dispersed fluorescence spectrum.[28] Consequently, if mode A is known in the ground state, it can be identified in the excited state.

The assignment of all prominent lines for *t*-stilbene excitation in Figs. 4 and 5 are tabulated in Table II. In Fig. 6 we have expanded the excitation spectrum of *t*-stilbene-h_{12} to help clarify the assignments of the many fundamentals and combination bands that follow. All assigned vibrations of S_1 are summarized and compared (where possible) to other work, calculations, the ground state modes (Table III), and the frequencies and vibronic intensities of styrene (Table IV).

Finally, we comment that excitation spectra offer far greater sensitivity than dispersed fluorescence spectra since *total* fluorescence may be collected in the former case. Furthermore, the resolution is limited by the laser bandwidth and not by the monochromator where resolution is obtained at the expense of sensitivity. The practical consequence is that the vibrational frequency determinations in S_1 (± 0.5 cm^{-1}) are generally more accurate than in S_0 (± 3 cm^{-1}).

1. Ethylene and low frequency modes in S_1

The excitation spectra in Figs. 4–6 exhibit a strong harmonic progression 25_0^m for the symmetric in-plane ethylene bend mode similar to the 25_n^0 progression observed in the 0^0 level dispersed fluorescence spectra (Figs. 1 and 2). Also similar to the ground state are the strong combinations formed by the ethylene ν_{25} mode with most other modes including benzene-type modes. Exciting into ν_{25} overtones (25_0^m), however, gives rise to a very different intensity distribution for the 25_n^m progression in the dispersed fluorescence spectra as seen in Fig. 7. Of particular note is the *absence* of the 25_1^1 band in the 25^1 level emission spectrum. One would expect this band to be the strongest for a small geometry change upon electronic transition. We examine the geometry changes that occur along the normal coordinate of ν_{25} by employing an extensive Franck–Condon analysis in Secs. IV A and IV B 1. An example of this analysis is given by the calculated 25_n^m intensity distributions in Fig. 7 for a geometry which best fits the data.

The SVL dispersed fluorescence are capable of clarifying some of the confusion which has arisen in the past regarding fundamentals whose frequencies are nearly coincident with the progression 25_0^m. SVL dispersed fluorescence spectra from pure S_1 fundamentals generally exhibit a 25_n^0 progression built onto a false origin (i.e., the first band in the progression is shifted from the excitation frequency by the frequency of the fundamental in S_0; see Fig. 3). Emission from a combination band involving m quanta of ν_{25}, on the other hand, will appear as a 25_n^m progression (Fig. 7) built on the false origin. An example of this is the 25_0^m progression in excitation which appears to extend to at least $m = 5$ in absorption and excitation spectra (Figs. 4–6). Under closer scrutiny, however, one finds that the apparent 25_0^3 band is overlapped with the strong fundamental $\nu_{23}[\nu_{6b}]$ (592.1 and 590.7 cm^{-1}, respectively in -h_{12}). The SVL dispersed fluorescence spectra for the two excitation bands are illustrated in Fig. 8. It is also straightforward to show then that the apparent 25_0^4 band at 789 cm^{-1} is actually due to the combination $23_0^1 25_0^1$ (Fig. 8).

Dispersed fluorescence spectra from various low frequency bands in S_1 are illustrated in Fig. 9. The spectra for $S_1 + 83$ and 95 cm^{-1} [Figs. 9(a) and 9(b)] are qualitatively similar indicating that they are strongly mixed bands. The mixing, however, does not appear to be due to Fermi resonance since, the first overtones to these bands occur at twice the frequency [Table II, Figs. 9(c) and 9(d)]. Overtones of modes perturbed by Fermi resonance occur at multiples of the unperturbed fundamental frequency indicating that the observed frequencies at 83 and 95 cm^{-1} are unperturbed. Judging by the number of strong bands in Figs. 9(a) and 9(b) that are otherwise weak in the 0^0 level fluorescence spectra (Figs. 1 and 2), it would appear that the two excited state bands may be described by a linear combination of several ground state modes (Table V). However, on the basis of relative intensities, the S_0 119 cm^{-1} band may be roughly associated with $S_1 + 83$ cm^{-1} and the 75 cm^{-1} band with $S_1 + 95$ cm^{-1}. A Franck–Condon analysis (Sec. IV B 2) is consistent with this premise. The very strong band at 266 cm^{-1} disappears in the $95 + 198(\nu_{25})$ cm^{-1} fluorescence spectrum. Since the 25_1^1 band vanishes due to Franck–Condon and geometry considerations (Fig. 7), the absence of the 266 cm^{-1} band is interpreted as being a combination band with ν_{25} in S_0, possibly corresponding to the combination $66 + 204$ cm^{-1}.

Weak excitation bands were also observed at 26, 39, 122, and 134 cm^{-1} which may correspond to certain ob-

Downloaded 21 Dec 2005 to 131.215.225.171. Redistribution subject to AIP license or copyright, see http://jcp.aip.org/jcp/copyright.jsp

Table II. Assignment of the Excitation Spectrum of trans-Stilbene.

t-Stilbene-h_{12}			t-Stilbene-d_{12}		
Frequency[a] (cm^{-1})	Relative Intensity[b]	Assignment[c,d]	Frequency[a] (cm^{-1})	Relative Intensity[b]	Assignment[c,d]
0.0	100	0_0^0	0.0	100	0_0^0
15.7	1.0	hot band	15.8	1.0	hot band
26.2	2.1		25.1	2.2	
38.6	3.3		36.3	3.4	
83.2	25	ν_{36}?	76.3	29	ν_{36} ?
95.1	26	ν_{37}?	87.2	25	ν_{37} ?
121.9	2.3	83 } +(39)	112.8	2.6	76 } +(36)
134.2	2.3	95 } +(39)	121.6	2.3	87 } +(36)
166.0	2.4	2×83	153.0	4.0	2×76
178.7	13.2	83+95	164.8	12.8	87+76
191.2	9.5	2×95	175.1	8.4	2×87
197.2	sh		180.6	7.8	
197.6	79	ν_{25}	187.9	69	ν_{25}
218.5	1.2		202.3	1.2	
224.6	10.5	198+(26) } *Fermi Resonance*	207.2	7.2	ν_{35} ?
228.6	6.1	ν_{35}? } *Fermi Resonance*	212.2	7.0	(25) } +188
236.7	4.0	198+(39)	224.9	4.0	(36) } +188
246.4	2.2	3×83	236.4	1.2	
262.7	2.3	2×83+95	241.6	3.2	2×76+87
274.8	4.8	2×95+83	252.6	4.6	2×87+76
280.3	30	$\nu_{24}[\nu_{9b}]$,198+83	256.4	1.8	
286.8	2.7	3×95	263.7	33	$\nu_{24}[\nu_{9b}]$, 188+76
292.4	25	198+95	274.9	21	188+87
319.5	2.8	(28) } +198+95	300.4	2.4	(25) } +188+87
331.6	2.6	(39) } +198+95	311.4	1.6	(36) } +188+87
363.0	4.4	2×83 }	341.1	18.4	oop fundamental
376.0	14	83+95 } +198	351.3	14.4	264+87
389.3	sh	2×95 } +198	362.6	7.2	2×87+188
389.8	13	oop fundamental	375.6	50	2×188
396.0	47	2×198 } *Fermi Resonance*	387.7	8.0	fundamental (b_u ?)
403.4	4.7	oop fund. } *Fermi Resonance*	394.1	11.2	oop fundamental
420.2	6.8	(28)+2×198	398.7	5.6	(25) } +2×188
425.1	sh	229+198	410.9	3.7	(36) } +2×188
425.9	6.9	fundamental (b_u ?)	428.1	6.9	2×76+87 } +188
434.1	3.6	(39)+198 }	438.6	7.6	2×87+76 } +188
459.0	4.0	2×83+95 }	451.2	23	264+188
471.5	8.1	2×95+83 } +198	461.8	11.9	2×188+87
478.1	23	280 }	473.3	10.8	oop fundamental
483.5	2.9	3×95 }	487.4	2.4	(25) } +×188+87
489.7	15	198+95 }	498.3	1.7	(36) } +×188+87
499.1	4.9	oop fundamental	527.0	21	341 } +188
516.1	4.1	(26) } +2×198+95	537.8	9.1	264+87 } +188
528.4	2.9	(39) } +2×198+95	549.3	3.9	2×87+2×188, 473+76
553.8	11.2	oop fundamental	562.0	24	3×188
			565.6	27	$\nu_{23}[\nu_{8b}]$
559.9	4.7	2×198+2×83 ?	572.4	7.1	388+188
567.7	3.6	2×95+83 }	579.9	8.2	$\nu_{22}[\nu_{8a}]$
572.4	10.2	198+83 } +198+95	590.5	5.4	(25) } +2×188
580.8	6.4	3×95 } +198+95	603.1	7.1	(36) } +2×188
585.2	sh	198+95 } +198+95	613.9	5.2	2×76+87 } +2×188
			638.0	10.8	76+188 } +2×188

Downloaded 21 Dec 2005 to 131.215.225.171. Redistribution subject to AIP license or copyright, see http://jcp.aip.org/jcp/copyright.jsp

TABLE II (*continued*).

585.7	9.6	fundamental ?
590.7	10(sh)	$\nu_{23}[\nu_{8b}]$
592.1	20	3×198
598.3	5.0	
617.8	8.1	(26)+3×198, (26)+591
621.7	7.2	$\nu_{22}[\nu_{8a}]$
630.2	1.0	(39)+198 } +2×198
655.7	2.1	2×83+95 } +2×198
662.5	8.1	oop fundamental
667.6	3.2	2×95+83 } +2×198
674.9	8.5	280 } +2×198
679.8	1.8	3×95 } +2×198
687.0	6.6	591+95, 3×198+95
695.9	3.9	499+198
717.1	8.2	oop fundamental
751.8	10.4	554 } +198
760.7	2.2	560 } +198
765.8	1.5	2×95+83 } +2×198+95
770.2	4.5	198+83 } +2×198+95
779.1	3.5	3×95 } +2×198+95
784.0	2.1	198+95 } +2×198+95
789.2	22	591+198, 4×198
821.1	6.1	622+198
845.8	17.4	} *Fermi Resonance*
849.3	17.4	$\nu_{21}[\nu_1]$ } *Fermi Resonance*
851.9	18.2	} *Fermi Resonance*
860.2	8.4	663+198
872.7	4.9	83 } +591+198
883.8	4.1	95 } +591+198
915.3	5.2	717+198
930.4	3.2	846 } +83
935.2	2.5	852 } +83
944.2	3.8	849 } +95
947.9	5.3	852 } +95
972.7	26	$\nu_{20}[\nu_{12}]$
987.3	13.3	591+2×198
994.9	4.0	$\nu_{19}[\nu_{18a}]$
1040.6	3.6	846 } +198
1045.0	17	849 } +198
1048.3	24	852 } +198
1055.9	3.8	972+83, 663+2×198 ?
1066.6	3.2	972+95
1069.8	5.0	$\nu_{18}[\nu_{18b}]$?
1129.3	1.0	849 } +198+83
1131.6	1.2	852 } +198+83
1140.3	1.5	849 } +198+95
1143.6	2.0	852 } +198+95
1165.7	1.8	972+2×95 ?
1170.3	13.1	$\nu_{15}[\nu_{13}]$? 972+198
1181.6	1.8	
1184.4	1.6	
1190.3	1.7	993+195
1237.4	7.5	846 } +2×198
1241.3	7.9	849 } +2×198
1245.9	8.5	852 } +2×198
1249.3	10.6	ν_{13}
1264.2	2.0	$\nu_{14}[\nu_3]$?
1270.0	2.5	1070+198 ?
1332.4	7.5	$\nu_{12}[\nu_{14}]$, 1249+83
659.7	13.0	474+188
713.6	9.5	2×76 } +3×188
736.0	2.6	2×87 } +3×188
741.3	8.0	$\nu_{19}[\nu_{18a}]$
747.7	7.6	4×188 } *Fermi Resonance*
753.6	27	566+188 } *Fermi Resonance*
778.3	6.2	$\nu_{18}[\nu_{18b}]$
829.5	11.2	$\nu_{21}[\nu_1]$?
859.0	9.5	$\nu_{16}[\nu_{9a}]$
866.8	3.0	$\nu_{17}[\nu_{15}]$?
906.8	4.0	754+2×76
928.5	6.2	741+188
934.3	27	$\nu_{20}[\nu_{12}]$
942.5	13.0	754+188
957.8	5.0	} $\nu_{14}[\nu_3]$?
969.6	6.2	} $\nu_{14}[\nu_3]$?
989.6	19.2	ν_{13}
990.5	19.2	ν_{13}
999.9	2.2	
1005.3	1.6	741+188+76
1011.8	3.4	934+76
1017.6	3.5	754+188+76
1022.2	2.9	934+87
1038.6	0.8	566+473
1044.0	1.1	958+87
1047.6	7.1	859+188, 660+388
1065.7	2.7	990+76
1077.6	1.8	990+87
1093.7	2.5	754+188+2×76
1113.2	2.2	
1121.0	3.5	934+188
1125.0	13.2	$\nu_{15}[\nu_{13}]$
1130.8	1.6	754+2×188
1143.9	1.0	2×572
1146.6	3.5	958+188
1155.2	1.5	
1157.0	3.3	970+188
1177.9	19.2	990+188
1199.5	3.5	1125+76
1212.0	1.7	1125+87
1224.7	2.1	660+566 ?
1234.9	3.6	859+2×188
1251.9	4.4	990+188+76
1253.7	4.4	990+188+76
1264.5	2.8	990+188+87
1274.9	2.0	2×76 } +1125
1288.1	2.2	87+76 } +1125
1300.5	0.8	2×87 } +1125
1306.7	2.0	$\nu_{11}[\nu_{18b}]$?, 566+741 ?
1311.3	2.9	1125+188
1319.4	1.0	2×660, 754+566, 754+3×188 ?
1330.4	1.9	990+188+2×76 } or 859+473
1333.5	1.8	970+2×188 } or 859+473
1339.4-1343.6	1.2	990+188+76+87
1365.1	8.8	990+2×188
1376.3	1.6	990+388
1383.9		

Downloaded 21 Dec 2005 to 131.215.225.171. Redistribution subject to AIP license or copyright, see http://jcp.aip.org/jcp/copyright.jsp

TABLE II (*continued*).

1342.5	3.1	1249+95 ?
1357.6	2.5	
1367.5	3.3	972+2×198
1377.6	2.0	
1387.0	2.0	
1401.6	1.6	
1418.3	1.9	
1429.7	1.8	$\nu_{11}[\nu_{19b}]$?
1434.1	2.7	846
1438.5	1.6	849 } +591
1442.2	3.1	852
1446.7	7.6	1249+198
1463.3	1.2	$\nu_{10}[\nu_{19a}]$?
1466.2	1.1	
1530.4	6.1	(1332) } +198
1542.3	3.1	(1343)
1548.4	3.5	$\nu_9[\nu_{8b}]$
1553.0	1.9	$\nu_8[\nu_{8a}]$?
1555.0	1.9	
1562.2	1.5	
1614.0	0.8	
1619.3	2.1	$\nu_8[\nu_{8a}]$?
1637.8	2.3	ν_7 ?
1643.6	3.2	1249+2×198
1720.2	1.3	
1725.8	2.6	(1332)+198
1737.8	0.5	(1343)+198 } +198
1744.2	2.5	(1548)
1753.2	1.0	
1759.8	0.9	
1810	0.5	(1614)
1819	1.1	(1619)
1834	0.7	(1638)
1839	1.0	(1249) } +2×198 } +198
1921	0.8	(1332)
1942	0.8	(1548)+198
1388.4	1.5	1125+188+76
1395.2	0.6	
1405.9	1.8	934+473
1440.4	2.3	990+2×188+76
1461.7	1.7	990+473
1494.1	7.2	754+741 ?
1500.7	11.9	934+566
1504.3	4.5	$\nu_9[\nu_{8b}]$
1522.4	2.9	$\nu_8[\nu_{8a}]$?
1537.4	2.0	
1554.5	2.1	990+566, 990+3×188 ?
1561.6	2.0	$\nu_8[\nu_{8a}]$?
1579.0	1.6	ν_7 ?
1611.5	0.6	859+754 ?
1615.2	0.6	
1626.6	0.9	
1631.5	0.5	
1679.4	6.8	
1685.2	7.1	3×566 ?
1691.1	1.9	
1709.1	4.6	
1743.2	2.0	990+754
1763.2	0.7	
1779.2	1.0	
1792.8	1.0	934+859
1816	1	
1841	1	
1846	1	
1863		
1866	2.5	2×934
1870		
1889		
1892	1	
1896		
1923	2	970+934
1933	1	

[a] Frequencies are reported relative to the 0_0^0 to an accuracy of 0.5 cm^{-1} or 0.1% (whichever is larger). [b] sh denotes shoulder, [c] See Table I, footnote c; [d] Rather than expressing modes in the notation for vibronic transitions, A_m^n introduced in Sec. III A and employed in Table. I, we use instead the frequencies of the fundamentals. See also Table I, footnote d.

served low frequency S_0 bands. However, there is evidence which suggests that some of these bands may be due to another rotomer of *t*-stilbene as discussed in Sec. IV D.

A fundamental has been identified in *t*-stilbene-h_{12} at 229 cm^{-1} (S_1) and 264 cm^{-1} (S_0) (Fig. 10) and is assigned as a C_e–φ out-of-plane mode of a_u symmetry (ν_{35}) for the following reasons: (i) agreement with IR/Raman work[16]; (ii) enhanced low frequency a_u bands in SVL fluorescence spectrum; and (iii) apparent Fermi resonance with the overall a_u combination at 198 + 26 cm^{-1} [Figs. 10(a) and 10(b)]. Excitation of the S_1 combination 229 + 198 (i.e., $35_0^1 25_0^1$) establishes the 264 cm^{-1} band as a fundamental since the 264 + 204 cm^{-1} emission band (i.e., $35_1^1 25_1^1$) is missing as expected for combinations involving the 25_1^1 transition (cf., Fig. 7). Note that this same criterion was used to identify the 266 cm^{-1} band in Fig. 9 as a combination involving ν_{25} and *not* the fundamental ν_{35}. A strong deuterium effect was observed which reduced the S_0 and S_1 frequencies to 231 and 207, respectively.

2. Benzene-type modes in S_1

a. In-plane vibrations. The use of SVL dispersed fluorescence spectra for identifying corresponding S_1 and S_0 modes is important since our knowledge of the S_1 vibrational modes is far less developed than for the ground state. Most of the lower frequency (i.e., < 1000 cm^{-1}) S_1 vibrations were assigned to a high degree of confidence in this manner. These include, e.g., ν_{16} through ν_{23} (Table III). Representative SVL

Downloaded 21 Dec 2005 to 131.215.225.171. Redistribution subject to AIP license or copyright, see http://jcp.aip.org/jcp/copyright.jsp

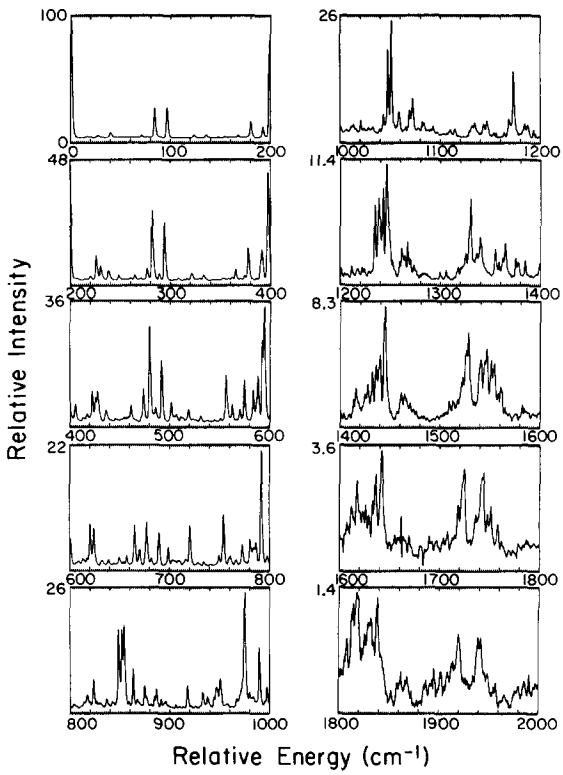

FIG. 6. Expanded view of the excitation spectra of t-stilbene-h_{12}. The spectra have been partitioned into 200 cm^{-1} segments to illustrate the strong progression and combination bands involving the 198 cm^{-1} mode ν_{25}. The wave number scale is approximate ($\pm$ 5 cm^{-1}). Expansion conditions were 50 psi He and 80 °C.

spectra are illustrated in Fig. 3.

The assignments of the high frequency vibrations are very uncertain since (i) the vibronic intensities in the excitation spectra decrease rapidly above the threshold energy ($\approx$1200 cm^{-1}) for isomerization; (ii) SVL dispersed fluorescence spectra at these energies are completely diffuse; and (iii) the large number of lines due to combinations makes it difficult to distinguish fundamentals. The strong lines at 1170 and 1125 cm^{-1} in t-stilbene-h_{12} and -d_{12}, respectively, are assigned to the C_e–φ stretch mode $\nu_{15}[\nu_{13}]$ on the basis of the ground state frequencies, the small deuterium effect, and the similarity with regard to frequency and vibronic intensity to the corresponding mode in styrene[4,26] (Table IV). The assignment of the $\nu_9[\nu_{8b}]$ and $\nu_{16}[\nu_{9a}]$ modes were made on the basis of a comparison with observed transient Raman signals in S_1 of solution phase t-stilbene.[29] Finally, the assignments of the relatively strong modes ν_{13}, $\nu_{20}[\nu_{12}]$, and $\nu_{23}[\nu_{6b}]$ are in accord with calculated vibronic intensities.[22]

We have identified an S_1 fundamental at 426 and 388 cm^{-1} for t-stilbene-h_{12} and -d_{12}, respectively, that corresponds to the much higher frequencies 565 (-h_{12}) and 521 (-d_{12}) cm^{-1} in the ground state (Fig. 11). Interestingly, these frequencies do not correspond to any previously reported a_g modes. The best agreement is found for the $\nu_{70}[\nu_{6b}]$, b_u mode reported[16] at 540 (h_{12}) and 520 (d_{12}) cm^{-1}, although the $\nu_{33}[\nu_{17b}]$ a_u mode at 526 (h_{12}) and 457 (d_{12}) are possibilities. An active b_u fundamental, however, would imply a C_i molecular geometry. The evidence presented in this paper is more consistent with C_2 geometry (Sec. IV C) in which case a_u modes can become active.

A pronounced example of Fermi resonance is exhibited by the three lines between 846–852 cm^{-1} in t-stilbene-h_{12} (Table II, Fig. 6). The excitation of the bands was resolvable. The resultant dispersed fluorescence spectra, which are illustrated in Fig. 12, are very similar except for the relative intensities of the low frequency intervals. We assign the active mode as $\nu_{21}[\nu_1]$. The three primary emission bands at 870, 889, and 910 cm^{-1} closely resemble the low frequency interval of 0, 20, and 44 cm^{-1} (e.g., Fig. 2). It is not clear why this interval, which is attributed to out-of-plane vibrations, is so strong in Fig. 12 nor is the source of the relative intensity differences known. It is possible that the band spacing is coincidental with the low frequency interval and may correspond instead to fundamentals.

b. Out-of-plane vibrations. A number of excitation bands were observed which correspond to out-of-plane (oop) benzene-type modes indicating that t-stilbene is nonplanar. The assignment of oop modes was made on the basis of the: (i) observation of strong fluorescence bands from these S_1 levels that were absent from the 0^0 level fluorescence spectrum; (ii) comparison of the fluorescence bands with oop modes assigned by Raman and IR work[16,18,25]; (iii) absence of strong in-plane a_g bands; and (iv) observed differences in the intensity distribution of the ν_{25} progression built onto in-plane and oop modes.

The determination of the symmetries of the oop bands as a_u (C_2 allowed) or b_g (C_i allowed) is not possible in these studies. We resort instead to a comparison of the observed band frequencies with symmetry assigned oop modes from Raman/IR work[16] in Table V. Typical examples of the dispersed fluorescence spectra from these S_1 levels are illustrated in Fig. 13. Most of the low frequency bands (i.e., from S_1 + 83 and 95 cm^{-1} excitation) have not been observed prior to this work and are discussed in greater detail in Secs. III C 1 and IV B 2. The higher frequencies, which correspond to benzene-type modes, correspond reasonably well with assigned a_u and b_g modes from previous work. In some instances, in-plane b_u modes may be associated with the observed bands; however, this may be due to coincidence since no a_g modes are apparent. The low frequency modes have been assigned for the most part as a_u and this symmetry is also consistent with the observed benzene-type modes. However, b_g activity is also discussed indicating that the nonplanarity of the molecule is probably not strictly C_2. The significance of the oop vibrations observed in this work with regard to the molecular geometry is discussed in Sec. IV C.

3. Vibrational Cooling

The vibrational cooling in jet expansions usually occurs to a different extent for different vibrational modes and is also dependent on the carrier gas and backing pressure. Consequently, weak features due to hot molecule absorptions (hot bands) can occur. In addition, weak complexes between seed and carrier molecules can occur which give rise to their own distinct absorptions. In order to distinguish weak features due to hot bands and complexes from the zero-point excitations of the molecule of interest, we recorded a series of excitation spectra under various expansion conditions. We illustrate some of these results in Fig. 14.

Downloaded 21 Dec 2005 to 131.215.225.171. Redistribution subject to AIP license or copyright, see http://jcp.aip.org/jcp/copyright.jsp

TABLE III. Assignment of the Totally Symmetric (a_g) Ground and Excited State Vibrations of t-Stilbene. Comparison with Calculations and other Work.

Mode No.[a]		Approximate Description[b]	Ground State h_{12} Calc.[c]	Ground State h_{12} Observed This Work	Ground State h_{12} Observed Ref. 16[d]	Ground State d_{12} Observed This Work	Ground State d_{12} Observed Ref. 16[d]	Excited State h_{12} Calc.[c]	Excited State h_{12} Observed This Work	Excited State h_{12} Observed Other Work[e]	Excited State d_{12} Observed This Work
1	[20b]	CH st	3092		3080		2294	3092			
2	[7b]	CH st	3090		3059		2284	3090			
3	[2]	CH st	3089		3052		2276	3080			
4	[13]	CH st	3088		3028		2268	3088			
5	[20a]	CH st (C_φ sens)	3087		3028		2256	3086			
6		C_φH st	3078		3013		2221	3078			
7		$C_\varphi C_\varphi$ st	1691	1654	1639	1613	1596	1671	1637.8 ?	1599	1579.0 ?
8	[8a]	CC st	1642	1607	1594	1573	1555	1606	1553.0 ?		1522.4 ?
9	[8b]	CC st	1599	1584 ?	1572	1549 ?	1535	1586	1548.4	1565[f]	1504.3
10	[19a]	CC st	1544	1495 ?	1494	1351-1380 ?	1368	1523	1463-66 ?		
11	[19b]	CC st + CCH ben	1511		1445		1324	1500	1429.7 ?	1427 ?	1306.7 ?
12	[14]	CCH ben + CC st	1464	1340	1339		1290	1460	1332.4		
13		$C_\varphi C_\varphi$H ben	1361	1321	1327	1023	1018	1321	1249.3	1337 ?	989.6 ?
14	[3]	CCH ben	1382		1315		1038	1392	1264.2 ?		969.6 ?
15	[13]	$C_\varphi\varphi$ st	1259	1208	1193	1152	1148	1264	1170.3 ?	1250	1125.0
16	[9a]	CCH ben	1174	1188	1187	872	869	1177		1177[f]	859.0 ?
17	[15]	CCH ben	1158	1162 ?	1156		840	1155		1144[f]	866.8 ?
18	[18b]	CCH ben	1085	1072	1059	828 ?	827	1086	1069.8 ?		778.3
19	[18a]	CCH ben	1043	1026	1027	786	798	1036	994.9		741.3
20	[12]	CCH ben + CC st + CCC ben	1051	1006	997	982	956	1041	972.7	978	934.3
21	[1]	$C_\varphi C_\varphi\varphi$ ben + CCC ben	930	870	854	847 ?		915	845.8-851.9	847	829.5 ?
22	[6a]	CCC ben (C_φ sens)	664	646	640	610	617	654	621.7	404	579.9
23	[6b]	CCC ben	713	624	617	592	593	700	590.7		585.6
24	[9b]	C_φCC ben	305	290	291	272	275	309	280.3		263.7
25		$C_\varphi C_\varphi\varphi$ ben	228	204	218	191	200	230	197.6	208	187.9

[a] Mode designations in brackets [ ] refer to benzene type modes according to Varsanyi's convention (Ref. 24). [b] Mode descriptions are adopted from Refs. 16 and 22. [c] Calculated frequencies are from Ref. 22. [d] Values were obtained by IR and Raman spectroscopy of powdered samples. [e] Values are from Ref. 15 unless otherwise noted. [f] Values are from transient Raman spectra of S_1; Ref. 29.

Spectra recorded under 50 psi of He (Fig. 14) gave the cleanest spectra in terms of the reduction of hot bands, bands due to possible rotomers (Sec. IV D) and van der Waals complexes. These features are clearly identified for expansions involving other carrier gases. Under 50 psi of Ar, hot bands and possible rotomer bands are easily recognized at -20, 39, and 134 cm^{-1} in Fig. 14. The absorptions at -41.4 and -63.9 cm^{-1} (i.e., to the red of the 0_0^0) are due to Ar–stilbene complexes which have been identified before.[14] Hot bands and rotomer bands are more prevalent in spectra recorded using N_2 as a carrier gas. Such behavior was also observed in the excitation spectra of anthracene[28] which has no low frequency modes and a substituted anthracene involving a large floppy group involving many low frequency modes.[3] The same situation is observed here, where it is evident that N_2 is not very effective in cooling the low frequency modes of *t*-stilbene. It should be realized, however, that very low frequency modes that display strong hot bands may still have vibrational temperatures that are lower than those for high frequency modes that exhibit only weak hot band intensities, owing to the energy difference term in the Boltzmann distribution. The identification of hot bands is important since these features not only occur at low energy, but show up in combination with higher frequency modes of the molecule (Table II). Spectra recorded with Ne as the carrier gas (not shown) gave essentially identical results with He. All excitation spectra used for vibrational assignments were recorded under 50 psi He, unless otherwise noted.

IV. ANALYSIS AND DISCUSSION

A. Franck–Condon analysis

The application of the Franck–Condon principle to the problem of determining excited electronic state structure in

Downloaded 21 Dec 2005 to 131.215.225.171. Redistribution subject to AIP license or copyright, see http://jcp.aip.org/jcp/copyright.jsp

TABLE IV. Comparison of ground and excited state vibrations and vibronic intensities of *t*-stilbene with styrene.

Mode No.[a]			*t*-Stilbene[b]		Styrene[b]	
			h_{12}	d_{12}	h_8	d_8
7		gnd	1654(20)	1613(30)	1600–1625(46)	1574
		exc	1637.8(2.3)?	1579.0(1.6)?	1608?	...
8	[8a]	gnd	1607(13)	1573(14)	overlapped	1563
		exc	1553.0(1.9)?	1522.4(2.9)?	with above	...
9	[8b]	gnd	1584(2.3)?	1549(5.1)?	1575	1536
		exc	1548.4(3.5)	1504.3(4.5)	...	...
10	[19a]	gnd	1495(2.8)?	1351(3.8) to 1380(4.3)?	1492(6.8)	1377
		exc	1463–66(1.7–1.8)?	...	1474	...
11	[19b]	gnd	1445	1324	1463(1.0)?	1327
		exc	1429.7(1.8)?	1306.7(2.0)?	1429	...
12	[14]	gnd	1340(6.8)	1290	1330(2.0)	1285
		exc	1332.4(7.5)	...	...	...
13		gnd	1321(5.1)	1023(11.2)	no corresponding	
		exc	1249.3(11)	989.6(19)	mode	
14	[3]	gnd	1315	1038	1282–1300(3)	1028
		exc	1264.2(2.0)?	969.6(6.2)?	1145.8(6.3)	...
15	[13]	gnd	1208(13)	1152(12)	1204(43)	1179
		exc	1170.3(13)?	1125.0(13)	1209.0(26)	...
16	[9a]	gnd	1188(4.2)	872(4.0)	1190(sh)?	870
		exc	...	859.0(9.5)?	980.7(3.1)?	...
17	[15]	gnd	1162(2.3)?	840	1156	841
		exc	...	866.8(3.0)?	965.4(8.3)?	...
18	[18b]	gnd	1072(3.8)	828(2.2)?	1084(15)	825
		exc	1069.8(5.0)?	778.3(6.2)	981–987(1.9–3.1)	...
19	[18a]	gnd	1026(4.6)	786(5.4)	996–1011(75)	841
		exc	994.9(4.0)	741.3(8.0)	959.1(23) or 947.8(23)	...
20	[12]	gnd	1006(11)	962(16)	same as	958
		exc	972.7(26)	934.3(27)	above	...
21	[1]	gnd	870(5.7)	847(2.7)?	779(14)	699
		exc	845.8(17)	829.5(11.2)?	745.8(24)	...
22	[6a]	gnd	646(3.5)	610(1.8)	433(4.4)	408
		exc	621.7(7.2)	579.9(8.2)	394.5(9.6)	...
23	[6b]	gnd	624(11)	592(14)	624(29)	594
		exc	590.7(10sh)	565.6(27)	523.2(4.6)	...
24	[9b]	gnd	290(5.8)	272(5.6)	227(2.0)	212
		exc	280.3(30sh)	263.7(33sh)	237.2(8.9)	...
25		gnd	204(71)	191(70)	no corresponding	
		exc	197.6(79)	187.9(69)	mode	

[a] See Table III, footnote a.

[b] All frequencies followed by parentheses ( ) are from this work for *t*-stilbene or Ref. 4 for styrene. sh denotes shoulder. The quantities in parentheses represent relative intensities with respect to the origin 0_0^0 intensity of 100. All other data are from Refs. 16 (*t*-stilbene ground state) and 26 (styrene).

simple polyatomic molecules has been reported previously.[30,31] We follow the general approach of Coon *et al.*[30] and Ansbacher.[31] The Franck–Condon factors $R(m, n)$ are calculated as a function of a distortion parameter γ along a normal coordinate, which we define as

$$\gamma = -\alpha' d\left(\frac{\beta}{1+\beta}\right)^{1/2}, \quad \beta = \frac{\alpha''}{\alpha'} = \frac{\nu''}{\nu'} \quad \alpha^2 = 4\pi^2\nu/h.$$

The ground and excited states are designated in the usual manner as n or $''$ and m or $'$, respectively. The term d is the

Downloaded 21 Dec 2005 to 131.215.225.171. Redistribution subject to AIP license or copyright, see http://jcp.aip.org/jcp/copyright.jsp

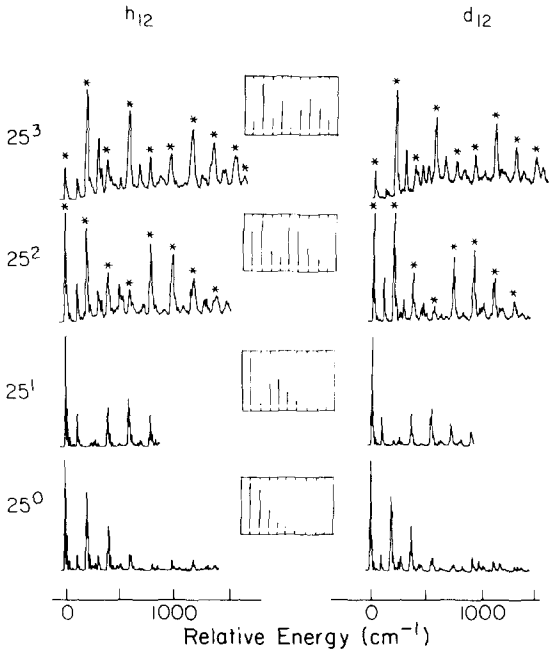

FIG. 7. SVL dispersed fluorescence spectra following excitation into the fundamental and overtones of the ν_{25} symmetric $C_eC_e\varphi$ in plane bend mode. The intensity distribution of the 25_n^m progressions were calculated for a series of geometry changes in *t*-stilbene using Franck–Condon analysis. The best fit to all spectra was obtained for a distortion parameter γ along the ν_{25} normal coordinate of 0.94. The calculated results for *t*-stilbene-h_{12} are illustrated in the inserts.

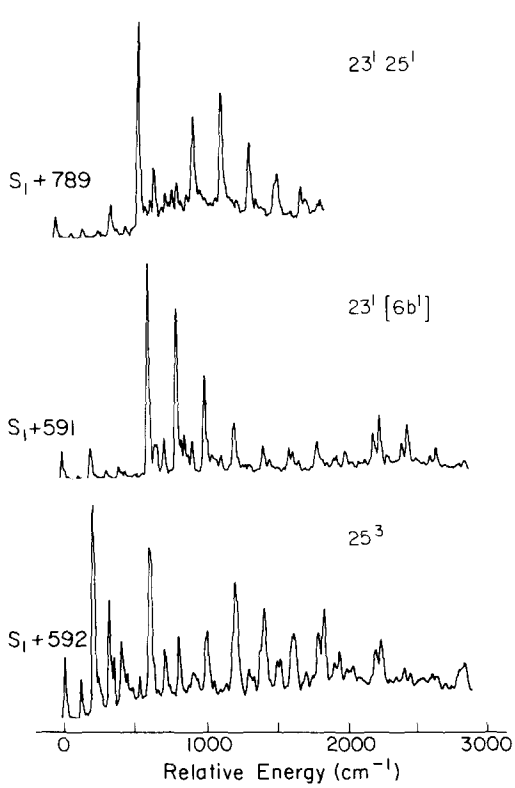

FIG. 8. The use of SVL fluorescence spectra to distinguish two strong overlapping lines in excitation. The lines at 591 and 592 cm^{-1} in the excitation spectrum of *t*-stilbene-h_{12} are clearly assignable as a benzene type fundamental $23^1[6b^1]$ and the 25^3 overtone of ν_{25}, respectively. The excitation line at 789 cm^{-1}, which appears to be the overtone 25^4 is actually due to the combination 23^125^1. This is confirmed by the appearance of the 25_n^1 intensity distribution (cf. Fig. 7) built onto the 23_0^1 false origin.

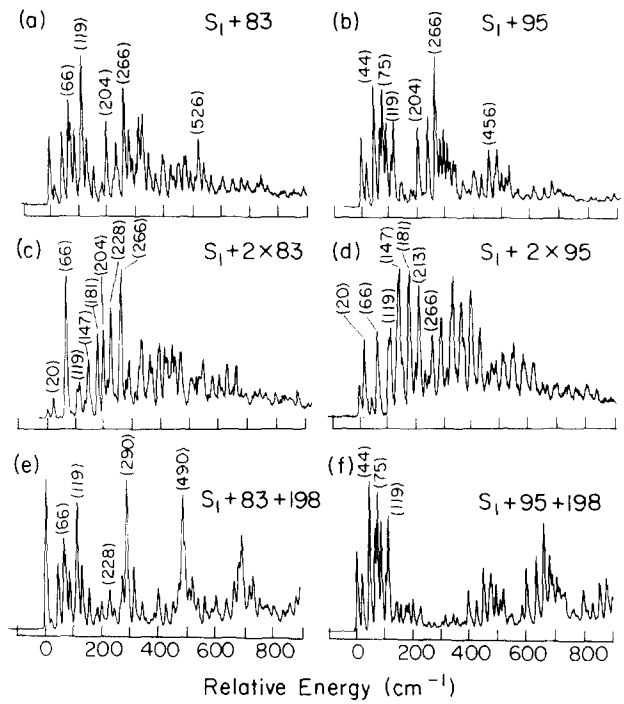

FIG. 9. SVL dispersed fluorescence spectra from S_1 levels at (a) 95 cm^{-1}; (b) 83 cm^{-1}; (c) 2×83 cm^{-1}; (d) 2×95 cm^{-1}; (e) $83+198$ cm^{-1}; and (f) $95+198$ cm^{-1}. Values in parentheses denote displacement in wave numbers from the excitation frequency.

change in the vibrational normal coordinate upon electronic transition (i.e., $d = q' - q''$) and is defined such that αd and therefore γ are dimensionless. For values of $\nu' \approx \nu''$, the distortion parameter γ is given approximately in units of the amplitude of one quanta of ν'' (i.e., $d \approx \gamma|\Delta q_{\max}| \approx 2^{1/2}\gamma|\langle\Delta q\rangle^2|^{1/2}$). We define the rms amplitude as $|\langle\Delta q\rangle^2|^{1/2}$. The relative spectral intensities are proportional to the square of $R(m, n)$.

B. Low frequency and torsional modes

1. Symmetric in-plane $\nu_{25}(a_g)$ bend mode: An unusual geometry induced interference effect

The ν_{25} vibration is the most optically active in *t*-stilbene and forms a long and smooth progression in both emission (25_n^0) and absorption (25_0^m) from the zero level of S_0 and S_1 (Figs. 1, 2, and 4–6, respectively). The intensity distribution of the progression in emission, however, changes drastically when exciting into the overtones of ν_{25} in S_1 as illustrated in Fig. 7. Most intriguing is the absence of the 25_1^1 band, which should be strong in the case where the S_1 geometry changes little from S_0.

The calculated Franck–Condon intensity distribution for emission from the first overtone of ν_{25} (i.e., 25_n^1) is illustrated in Fig. 15 as a function of the distortion parameter γ. The 25_1^1 band is clearly shown to vanish for $\gamma \approx 1.0$. This corresponds to a geometry change between S_0 and S_1 in which the vibrational wave functions for one quantum of ν_{25} interfere completely to give zero vibronic overlap as observed. The calculated intensities of the other bands in the 25_m^1 progression are also in excellent agreement with obser-

Downloaded 21 Dec 2005 to 131.215.225.171. Redistribution subject to AIP license or copyright, see http://jcp.aip.org/jcp/copyright.jsp

TABLE V. Out-of-plane vibrations observed in SVL dispersed fluorescence spectra.

h_{12}			d_{12}		
Excited state	Ground state	Ref. 16[a]	Excited state	Ground state	Ref. 16[a]
	20(13)[b]			17(6)	
	44(56)			40(54)	
	66(44)				
83	75(30)		76	65(67)	
(25)[b]	90(44)		(29)[b]	80(28)	
	119(100)	108, ν_{48}–b_g		105(100)	100, ν_{48}–b_g
	526(35)	526, $\nu_{33}[\nu_{17b}]$–a_u		451(24)	457, $\nu_{33}[\nu_{17b}]$–a_u
	20(31)			17(17)	
	44(89)			40(83)	
	66(15)				
95	75(100)[c]		87	65(100)	
(26)	90(46)		(25)	80(44)	
	119(77)	108, ν_{48}–b_g		105(58)	100, ν_{48}–b_g
	456(46)	455, $\nu_{34}[\nu_{16a}]$–a_u		425(22)	429, $\nu_{34}[\nu_{16a}]$–a_u
				451(39)	457, $\nu_{33}[\nu_{17b}]$–a_u
	119(32)	108, ν_{48}–b_g		105(36)	100, ν_{48}–b_g
	179(28)			159(39)	
	246(33)	239, $\nu_{47}[\nu_{10b}]$–b_g			
229			207		267, ν_{35}–a_u
(6.1)	265(100)	268, ν_{35}–a_u 262, ν_{72}–b_u	(7.2)	231(100)	259, ν_{72}–b_u 230, $\nu_{36}[\nu_{16b}]$–a_u
	418(42)	410, $\nu_{45}[\nu_{16a}]$–b_g		364(39)	408, $\nu_{45}[\nu_{16a}]$–b_g
	550(21)	526, $\nu_{33}[\nu_{17b}]$–a_u 540, $\nu_{70}[\nu_{6b}]$–b_u		480(32)	457, $\nu_{33}[\nu_{17b}]$–a_u 520, $\nu_{70}[\nu_{6b}]$–b_u
	119(63)	108, ν_{48}–b_g		105(28)[d]	100, ν_{48}–b_g
390	246(23)	239, $\nu_{47}[\nu_{10b}]$–b_g	341	217(44)	207, $\nu_{47}[\nu_{10b}]$–b_g
(13)	418(100)	410, $\nu_{45}[\nu_{16a}]$–b_g	(18)	368(100)	408, $\nu_{45}[\nu_{16a}]$–b_g
	451(47)	455, $\nu_{34}[\nu_{16a}]$–a_u		385(25)	429, $\nu_{34}[\nu_{16a}]$–a_u
	526(31)	526, $\nu_{33}[\nu_{17b}]$–a_u			
				233(65)[d]	see 267,259, 230 above
403	418(100)	410, $\nu_{45}[\nu_{16a}]$–b_g	394	348(70)	335, $\nu_{46}[\nu_{16b}]$–b_g
(4.7)	574(75)	540, $\nu_{70}[\nu_{6b}]$–b_u	(11)	424(100)	408, $\nu_{45}[\nu_{16a}]$–b_g
				476(38)	457, $\nu_{33}[\nu_{17b}]$–a_u
499	457(100)	455, $\nu_{34}[\nu_{16a}]$–a_u 467, $\nu_{71}[\nu_{9b}]$–b_u			
(4.9)	612(85)	612, $\nu_{44}[\nu_4]$–b_g			
	265(81)	268, ν_{35}–a_u		230(80)	see above
	420(62)	410, $\nu_{45}[\nu_{16a}]$–b_g		365(66)	408, $\nu_{45}[\nu_{16a}]$–b_g
554	526(14)	526, $\nu_{33}[\nu_{17b}]$–a_u	473	467(17)[e]	457, $\nu_{33}[\nu_{17b}]$–a_u
(11)	538(16)	540, $\nu_{70}[\nu_{6b}]$–b_u	(11)		
	612(100)	612, $\nu_{44}[\nu_4]$–b_g		532(100)	541, $\nu_{44}[\nu_4]$–b_g
	668(55)	675, $\nu_{69}[\nu_{6a}]$–b_u		583(39)	598, $\nu_{69}[\nu_{6a}]$–b_u
	680(65)	691, $\nu_{32}[\nu_4]$–a_u			645, $\nu_{32}[\nu_4]$–a_u
	267(10)	268, ν_{35}–a_u			
	456(43)	455, $\nu_{34}[\nu_{16a}]$–a_u 467, $\nu_{71}[\nu_{9b}]$–b_u			
662	613(50)	612, $\nu_{44}[\nu_4]$–b_g			
(8.1)	678(29)	675, $\nu_{69}[\nu_{6a}]$–b_u 691, $\nu_{32}[\nu_4]$–a_u			
	801(100)	...			
	868(14)	842, $\nu_{42}[\nu_{10a}]$–b_g 845, $\nu_{30}[\nu_{10a}]$–a_u			

Downloaded 21 Dec 2005 to 131.215.225.171. Redistribution subject to AIP license or copyright, see http://jcp.aip.org/jcp/copyright.jsp

TABLE V (*continued*).

	520(44)	526, $\nu_{33}[\nu_{17b}]-a_u$
	531(50)	540, $\nu_{70}[\nu_{6b}]-b_u$
717	667(75)	675, $\nu_{69}[\nu_{6a}]-b_u$
(8.2)	680(81)	691, $\nu_{32}[\nu_4]-a_u$
	867(88)	840, $\nu_{68}[\nu_1]-b_u$
	878(100)	842, $\nu_{42}[\nu_{10a}]-b_g$
		845, $\nu_{30}[\nu_{10a}]-a_u$

[a]Frequencies represent near lying modes and do not necessarily imply an assignment with the present work.
[b]Intensities given in parentheses are relative to the 0_0^0 in the excitation spectra and to the strongest peak in the SVL dispersed fluorescence spectra. In the case of overlapping lines, an estimation of the true intensities and not the peak heights are reported.
[c]The strongest band is actually due to a combination band at 266 cm^{-1} [see Fig. 9(b)].
[d]The relative intensities are from SVL fluorescence spectra following excitation of the S_1 fundamental + ν_{25} band.
[e]The 467 cm^{-1} band becomes very prominent in the $S_1 + 473 + 188$ cm^{-1} dispersed fluorescence spectrum.

vation (Fig. 7). Extending the analysis to higher overtone excitation also gave excellent agreement with experiment. The best fit to all spectra was obtained for a distortion parameter along the ν_{25} normal coordinate of $\gamma = 0.94$. We summarize the calculated and observed intensity distributions, normalized to the 0_0^0, in Table VI.

The distortion parameter γ is in approximate units of the vibrational amplitude, hence, it is possible to estimate the change in geometry along the normal coordinate of ν_{25} that occurs upon electronic excitation. The calculated motion of the ν_{25} mode[32] is given by

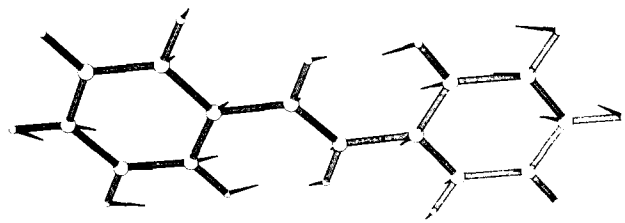

which approximately represents a $C_eC_e\varphi$ symmetric in-plane bend (the arrows are approximately 15 times greater than the actual amplitudes). We define the bend angle

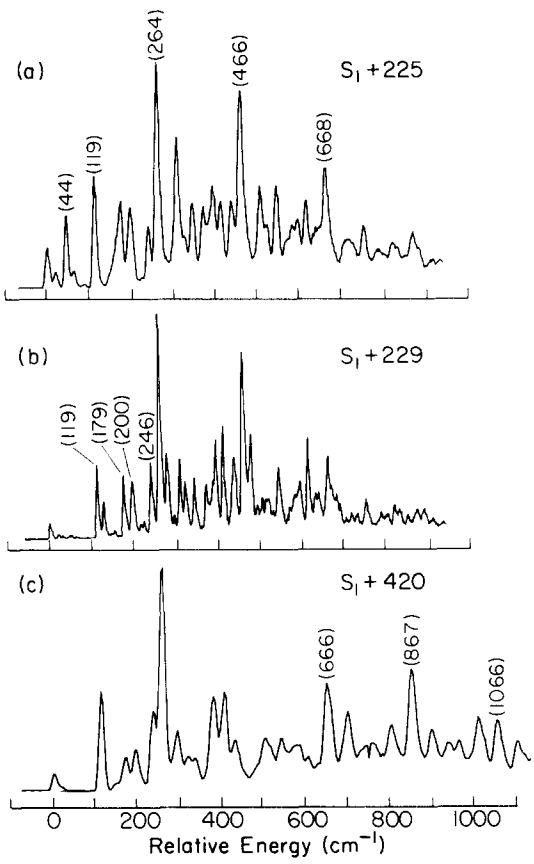

FIG. 10. Dispersed fluorescence spectra from S_1 levels at (a) 225 cm^{-1}; (b) 229 cm^{-1}; and (c) 420 cm^{-1}. The similarity of the $S_1 + 225$ and 229 cm^{-1} spectra is indicative of Fermi resonance. A frequency perturbation is apparent in that the $S_1 + 420$ cm^{-1} spectrum, which is assigned to the 225 + 198 cm^{-1} combination, does not appear at the sum frequency.

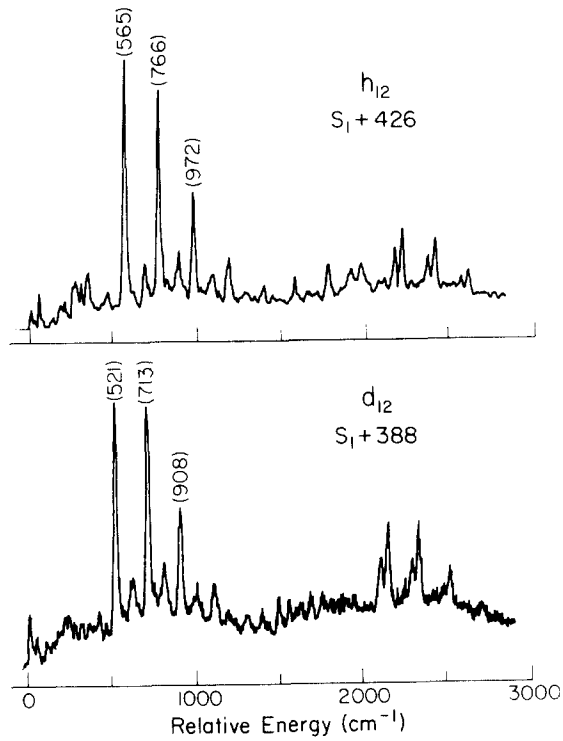

FIG. 11. Examples of large shifts in the fundamental frequencies of vibrations in S_0 and S_1. Fluorescence spectra are illustrated for *t*-stilbene-h_{12} and -d_{12}.

Downloaded 21 Dec 2005 to 131.215.225.171. Redistribution subject to AIP license or copyright, see http://jcp.aip.org/jcp/copyright.jsp

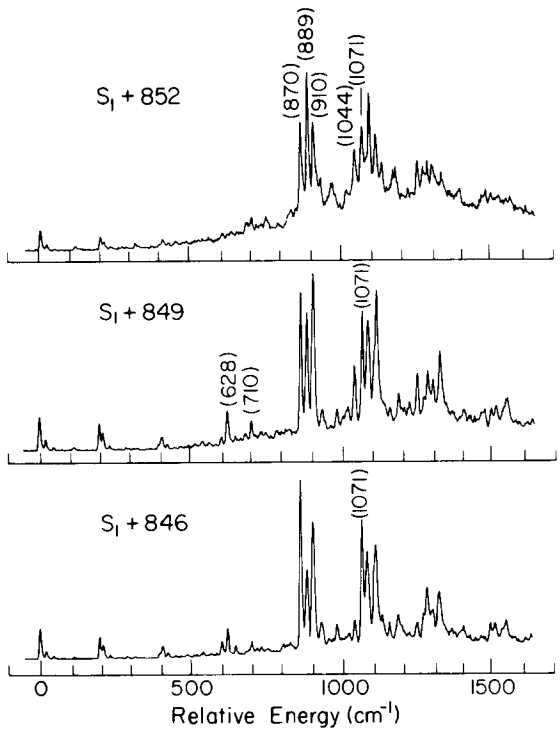

FIG. 12. SVL fluorescence spectra from the closely spaced bands at $S_1 + 846$, 849, and 852 cm^{-1}. The similarity of the spectra is evidence of strong mixing, presumably due to Fermi resonance.

through the center of the phenyl group to account for bending of the $C_eC_1C_2$ angle (where C_1 and C_2 are phenyl carbons). By combining the observed Franck–Condon factors with a normal mode analysis[32,33] the difference in this bend angle in S_0 and S_1 is calculated to be $1.3 \pm 0.3°$. The amplitude of this internal bend coordinate for the symmetric ν_{25} bend mode for one quanta in S_0 is $|\langle \Delta\varphi \rangle^2|^{1/2} = 1.0 \pm 0.2°$. The increase in the bond angle in S_1 is presumed to be due to the delocalization of double bond character from the ethylene C_e–C_e bond to C_e–φ bond.

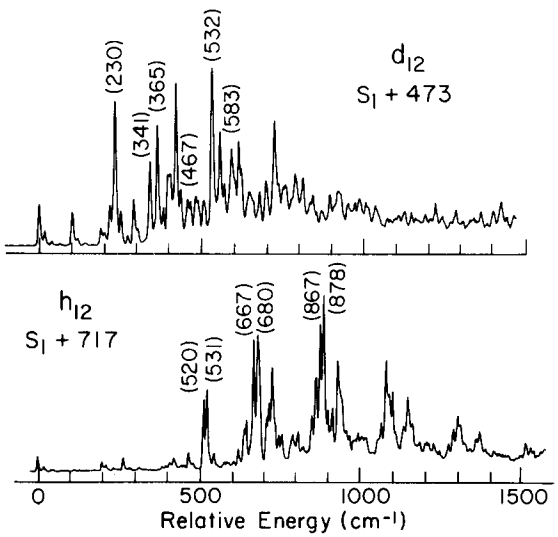

FIG. 13. Examples of fluorescence spectra from out-of-plane S_1 vibrations. These spectra are characterized by the variety of strong emission bands that are not present following in-plane S_1 vibronic excitation and the unusual intensity distribution observed for the 25_n^0 progression.

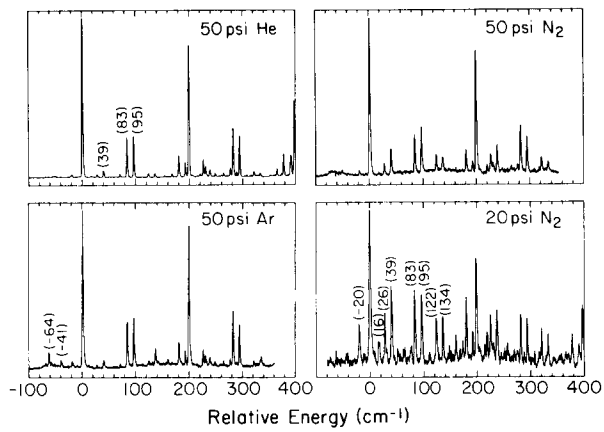

FIG. 14. Excitation spectra of *t*-stilbene-h_{12} for various carrier gases. The spectrum corresponding to 20 psi N_2 was recorded using ionization detection, hence the relative intensities are not expected to correlate with the other spectra recorded using fluorescence detection. Sample temperature was 80 °C.

2. Low frequency out-of-plane modes

A definitive assignment of the low frequency modes in S_0 and S_1 is clouded for the reasons that: (i) there is a large change in the vibrational coordinates and frequencies upon electronic excitation; (ii) there appear to be more low frequency components than indicated by the calculations[22]; (iii) previous spectroscopic studies[15–19,23] were unable to reveal the low frequency S_0 bands; and (iv) there is no conclusive way to ascertain the symmetry of the observed vibrations. The question of symmetry is an important one since it provides information on the equilibrium geometry of the molecule in the ground and excited electronic state. There are no obvious indications of nontotally symmetric modes (e.g., enhanced intensities for even overtones). However, the calculated frequencies by Warshel[22] indicate that only a_u vibrations have frequencies below 80 cm^{-1}.

We tentatively assign the 83 and 95 cm^{-1} modes to the

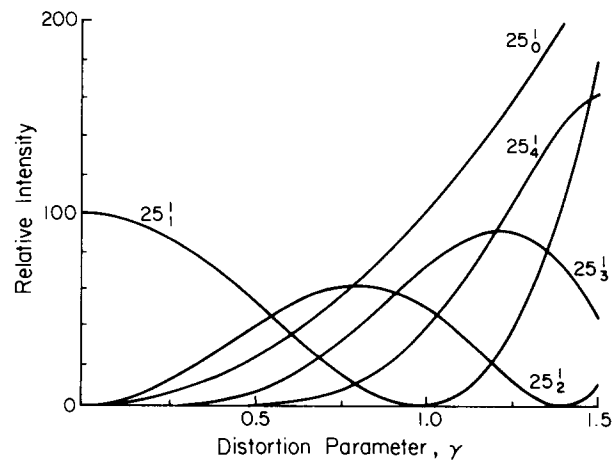

FIG. 15. Calculated Franck–Condon fluorescence intensity distribution for the 25_n^1 progression. The parameter γ denotes the change in the ν_{25} normal coordinate that occurs upon $^1B_g \leftrightarrow {}^1A_g$ electronic transition. The calculation applies to *t*-stilbene-h_{12} using the ground and excited state frequencies $\nu''_{25} = 204$ cm^{-1} and $\nu'_{25} = 198$ cm^{-1}. Essentially identical results were obtained using the frequencies for the -d_{12} isomer.

Downloaded 21 Dec 2005 to 131.215.225.171. Redistribution subject to AIP license or copyright, see http://jcp.aip.org/jcp/copyright.jsp

TABLE VI. Franck–Condon analysis of the ν_{25} mode. Comparison of calculated and observed intensity distribution in excitation and SVL dispersed fluorescence spectra for *t*-stilbene-h_{12}.

m \ n	Relative intensities[a,b] 0	1	2	3	4	5	6	7	8
0	100	89	42	14	4	1	0	0	0
	(100)[c]	(71)	(28)	(14)	(5)				
1	94	1	50	58	32	12	3	1	0
	(79)	(0)	(29)	(36)	(24)	(12)			
2	42	58	17	11	47	43	22	8	2
	(47)	(39)	(19)	(10)	(31)	(28)	(15)	(8)	
3	12	64	16	38	0	27	44	31	14
	(20)	(72)	(22)	(52)[d]	(18)[d]	(22)	(38)	(28)	(18)

[a]Calculated intensities $R(m, n)^2$ are for a distortion parameter along the ν_{25} normal coordinate of $\gamma = 0.94$. Values in parentheses are observed relative intensities.

[b]The rows and columns designate dispersed fluorescence and excitation spectra, respectively. The observed values for $A_n^m = 25_0^m$ are from excitation spectra and are used to normalize the observed relative intensities in fluorescence.

[c]Since the observed 0_0^0 has intensity due to other modes besides ν_{25}, the observed relative intensity of the 0_0^0 with respect to the ν_{25} progression will be larger than predicted by the calculations.

[d]The discrepancy between observed and calculated intensities is due to overlapping lines from the $S_1 + 591$ cm^{-1} fundamental (see Figs. 7 and 8).

C_e–φ bend ν_{36} and C_e–φ torsion, ν_{37}, modes of a_u symmetry for the following reasons:

(i) Warshel[22] calculates that these modes occur at 55 and 41 cm^{-1}, respectively, and that their vibronic intensity for C_2 molecular geometry (6° oop phenyl rotation) is 0.22 and 0.65 of the 0_0^0. The large values are perhaps indicative of the strong effect that these motions have on the overlap of the π orbitals. Our reason for reversing the order of the assignments compared to Warshel's frequencies is based on the association of the S_1 modes with those in S_0 which we discuss shortly.

(ii) The 83 and 95 cm^{-1} modes in S_1 are strongly mixed among the corresponding S_0 normal coordinates (Sec. III C 1). This indicates that significant geometry changes take place along these normal coordinates as a result of electronic excitation. It has already been shown that the C_e–C_e–φ angle undergoes a large change in S_1, presumably due to delocalization of ethylene double bond character into the C_e–φ bond. The same behavior was observed for the C_e–φ torsion and bend modes in the related molecule styrene.[4,26,27]

(iii) The dispersed fluorescence spectra from $S_1 + 83$ and 95 cm^{-1} are similar (Fig. 9) and give rise to very strong emission bands that are otherwise weak in the 0^0 level spectrum (Figs. 1 and 2), indicating that the symmetry of these modes are the same but not a_g.

(iv) In benzophenone, where C–φ torsion and bend modes similar to stilbene are expected, observed frequencies of 90 and 102 cm^{-1} for the excited and ground state, were reported.[34]

One other possibility for the appearance of the 83 and 95 cm^{-1} modes (or other nontotally symmetric modes) is through vibronic coupling with a near lying excited state of A_u (b_g induced) or A_g (b_u induced) symmetry. The A_g states, however, are not one-photon active[20,35] and hence are not expected to contribute oscillator strength through vibronic coupling. An example of vibronic intensity borrowing, possibly involving a low lying A_u state, was reported for the related molecule diphenylbutadiene.[5] In *t*-stilbene, the lowest lying A_u state is predicted to occur at about 20 000 cm^{-1} above the S_1 B_u state.[20] Unless there is an unusually strong interaction, A_u states are not expected to contribute significant intensity borrowing. We have measured the fluorescence decay times from all the observed low frequency S_1 modes (see the following paper[8]) and find that they are the same as those measured for all other modes below the reaction barrier (< 1200 cm^{-1}). This, unlike the situation found in diphenylbutadiene,[5] indicates that the low frequency modes are more likely to belong to the B_u state than to be vibronically induced.

We have calculated the Franck–Condon intensities for a range of geometry changes by associating the S_0 bands at 20, 44, 75, and 119 cm^{-1} to the S_1 bands at 83 and 95 cm^{-1}. This method is very qualitative since we consider single S_0 modes in spite of the mixed nature of the S_1 vibrations. We also treat these modes as totally symmetric for some reduced molecular symmetry group. In Table VII we summarize the results for various situations which compare the best calculated geometry dependent fit to the observed relative intensities of the corresponding modes in S_0 [Figs. 9(a)–9(d)] and S_1 (Fig. 6). The analysis was carried out to only two quanta (i.e.,

TABLE VII. Franck–Condon analysis of low frequency modes.

	m \ n	Relative intensity[a] 0	1	2	3
(A)	0	100	7	9	
		(100)	(12)	(–)	
$\nu' = 83$ cm^{-1}					
$\nu'' = 119$ cm^{-1}	1	14	71	5	
$\gamma = 0.20$[b]		(25)	(53)	(–)	
	2	2	28	43	
		(2)	(9)	(24)	
(B)	0	100	8	1	
		(100)	(2)	(–)	
$\nu' = 95$ cm^{-1}					
$\nu'' = 75$ cm^{-1}	1	5	84	17	
$\gamma = 0.25$		(26)	(54)	(9)	
	2	3	7	67	
		(9.5)	(–)	(50)	
(C)	0	100	16	11	8
		(100)	(8)	(–)	(–)
$\nu' = 95$ cm^{-1}					
$\nu'' = 44$ cm^{-1}	1	4	49	25	16
$\gamma = 0.50$		(26)	(47)	(35)	(9)
	2	22	0	10	16
		(9.5)	(5)	(–)	(–)

[a]Values in parentheses are observed relative intensities; see also footnote b in Table VI.

[b]The distortion parameter γ applies to individual normal coordinates only.

Downloaded 21 Dec 2005 to 131.215.225.171. Redistribution subject to AIP license or copyright, see http://jcp.aip.org/jcp/copyright.jsp

$n, m = 0$–2) since these were all that could be seen in the observed spectra. The most consistent agreement was obtained when the S_0 modes at 75 and 119 cm^{-1} were associated with the S_1 modes at 83 and 95 cm^{-1}. On the basis of the relative proportions of the ground state bands in the dispersed fluorescence spectra from $S_1 + 83$ and 95 cm^{-1} [Figs. 9(a) and 9(b)], we can roughly associate the 83 and 95 cm^{-1} modes with the ground state frequencies 119 and 75 cm^{-1}, respectively.

The calculated Franck–Condon intensity distributions proved inconsistent with the observed spectra for any geometry when the assumed S_0 fundamentals at 20 and 44 cm^{-1} were associated with the excited state bands at 83 and 95 cm^{-1}. The large frequency difference between the S_0 and S_1 bands gives rise to an alternating intensity pattern as illustrated in Table VII C for the pairing of frequencies 44 and 95 cm^{-1}. This effect is even more pronounced for calculations which paired the 20 and 95 cm^{-1} S_0 and S_1 modes. In fact, an alternating intensity pattern may be discernible in Figs. 9(a)–(d) if we assume that bands in approximate multiples of 20 cm^{-1} are overtones. However, the phase of the alternation is opposite to that calculated.

It is possible that the weak S_1 bands at 26 and 39 cm^{-1} are fundamentals associated with the ground state bands at 20 and 44 cm^{-1}. The 26 and 39 cm^{-1} bands exhibit interesting features. Their intensities vary significantly with the cooling condition of the jet expansion as illustrated in Fig. 14, yet they are probably not hot bands as indicated by the absence of bands shifted to the blue of the excitation energy in the dispersed fluorescence spectra (Fig. 16). Evidence discussed in Sec. IV D suggests that these bands correspond to another rotomer. However, the possibility of fundamentals is not ruled out. For instance, the 39 cm^{-1} band appears to have a weak overtone and to form combinations with the 83 and 95 cm^{-1} bands [Fig. 14(d)], thus suggesting that this band is a fundamental. Likewise, there appears to be a Fermi resonance between the 26 + 198 and the 229 cm^{-1} bands (Fig. 10). A possible explanation for these effects is a potential surface and hence vibronic intensities that are dependent on rotational energy.

C. Molecular geometry

The question of the *t*-stilbene geometry has been the focus of many studies,[17–19] however, the answer is still uncertain. Evidence suggests that the molecule is essentially planar (C_{2h}) in crystals,[36] but distorts in the solution and vapor phase by an out-of-plane (oop) twist of the phenyl groups. There are two ways in which this may occur; via in-phase (i.e., parallel) or out-of-phase rotation of the phenyl groups. The former geometry is described by the C_i group (where a_g of C_i transforms like a_g and b_g of C_{2h}) and induces 0^0 level vibronic activity for b_g type modes. The latter case, on the other hand, corresponds to C_2 symmetry (where a of C_2 transforms like a_g and a_u of C_{2h}) which allows a_u type modes to be observed.

An electron diffraction study indicated that the rms twist angle of the phenyl groups in *t*-stilbene is about 30°.[37] However, the rms angle does not necessarily correspond to the equilibrium angle, but may instead represent the rms displacement of a large amplitude torsional motion from an

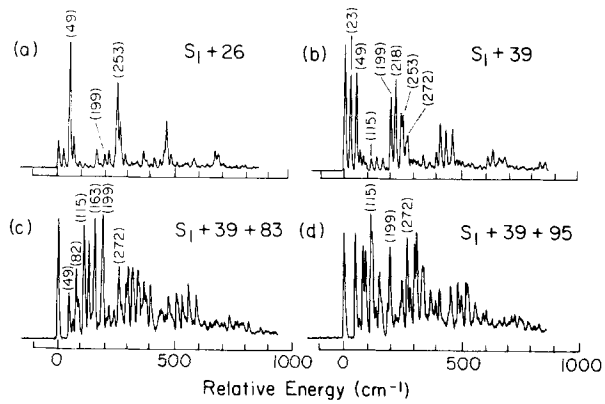

FIG. 16. Dispersed fluorescence spectra from the S_1 excitation bands at (a) 26 cm^{-1}; (b) 39 cm^{-1}; (c) 39 + 83 cm^{-1}; and (d) 39 + 95 cm^{-1}. The frequencies and relative intensities observed in these spectra indicate that the excitation bands may correspond to another rotomer.

equilibrium planar geometry. If we assume that the latter possibility is unreasonable, then the electron diffraction study is consistent with a C_2 geometry. A similar conclusion was reached in a photoelectron study.[38] IR and Raman studies are also in support of this conclusion[17] by detecting the appearance of C_2 allowed symmetry vibrations in the transition from solid *t*-stilbene to a melt. Some uncertainty is present, though, since the symmetry of the modes observed are not completely established. Warshel,[22] on the other hand, favors a C_i geometry on the basis of two absorption lines observed in an earlier study[15] which he assigns to calculated b_g modes. However, one of these lines is absent in our jet-cooled spectra and the other line is attributable to a combination band involving a previously undetected low frequency mode. Another study also reports the observation of a b_g vibration[19] implying C_i geometry, however, the symmetry assignment cannot be considered conclusive.

Naturally, the observation of nontotally symmetric out-of-plane modes plays a strong role in assessing the nonplanarity of *t*-stilbene. As in previous studies, we cannot positively distinguish between a_u and b_g modes. We do, however, observe many low frequency modes in both excitation and emission that were not previously observed. The calculations of Warshel also indicate that only a_u modes have frequencies below 80 cm^{-1}. One might intuitively expect a_u modes to have lower frequencies than b_g modes. The former vibrations involve out-of-phase motions of the phenyl groups. For a torsion, this would involve phenyl rotations opposite to each other corresponding to a large relative displacement of large masses. The in-phase motion, on the other hand, involves very little relative displacement of the phenyl groups; in fact, the motion is best described by twisting the ethylene group. Since, in-phase (b_g) motion involves predominantly the lighter ethylene group, its frequency should be higher than out-of-phase motion (a_u) involving large phenyl displacements. Our observation of very low frequency modes, particularly in S_0, is therefore consistent with a_u vibrations and a C_2 molecular geometry.

We have also observed oop vibrations which correspond to modes which have been assigned in previous studies[16,18,23] as a_u and b_g (Table V). Still in question then is whether a highly distorted geometry of symmetry less than either C_2 and C_i exists, in which case all modes would be

Downloaded 21 Dec 2005 to 131.215.225.171. Redistribution subject to AIP license or copyright, see http://jcp.aip.org/jcp/copyright.jsp

somewhat allowed. This would occur, for instance, if the phenyl twist angles were not equivalent. Finally, more than one rotomer may be stable thus accounting for some of the past confusion regarding the geometry. We consider this latter possibility next.

D. Possibility of rotomers for *t*-stilbene

The 26 and 39 cm^{-1} band intensities are strongly dependent on the jet beam cooling conditions (Fig. 14). Hot bands can be ruled out since the dispersed fluorescence spectra from these levels (Fig. 16) do not show any emission to the blue of the excitation frequency nor do the spectra resemble any that were recorded from known levels in S_1. It is conceivable that the 26 and (particularly) the 39 cm^{-1} bands represent another rotomer of *t*-stilbene. In Fig. 16 we present the SVL dispersed fluorescence spectrum from the 26 and 39 cm^{-1} levels in S_1, as well as from the 39 + 83 and 39 + 95 cm^{-1} bands. We make note of some important features in the S_1 + 39 cm^{-1} spectrum; (i) the spectrum qualitatively resembles a 0^0 level spectrum such as Fig. 2; (ii) the relative intensities of the low frequency bands are much larger than that observed in fluorescence spectra from other excited state levels; and (iii) the frequencies of many ground state modes are slightly different than those observed in the dispersed fluorescence from other levels (e.g., the 0^0 level; cf. Figs. 1, 2, and Table VIII).

The observations in Fig. 16 may be interpreted as evidence for another rotomer of *t*-stilbene. A different geometry would not only account for changes in the frequencies but also in the relative intensities by altering the allowedness of the out-of-plane a_u and b_g vibrations. We assume that the 39 cm^{-1} band is the 0^0 level of the less favored rotomer and compare the two sets of observed frequencies in Table VIII. The lowest frequency band is observed to increase from 20 to 23 cm^{-1} in going to the less favored rotomer. That this difference is real is attested to by the hot bands observed in Fig. 14 for the major 0_0^0 band at -20 cm^{-1} and for the 39 cm^{-1} (minor 0_0^0) at 16 cm^{-1} (i.e., $-23 = 16$–39 cm^{-1}). In previous studies in solution, it was suggested that more than one rotomer of *t*-stilbene may exist on the basis of asymmetric S_1 transient Raman band shapes[29] and certain effects observed in transient absorption spectra.[39] However, the determination of the geometries of the different rotomers was not possible.

It is tempting to attribute the unfavored rotomer to a C_i geometry, however, no new modes that might have b_g symmetry are apparent. Instead, the geometry appears to be C_2 but further distorted from planarity than the preferred rotomer judging by the strength of the lowest frequency bands (Fig. 16). Other indications consistent with a larger phenyl twist angle are the decreased frequency of the ν_{25} symmetric in-plane bend mode[17(a)] and the slightly higher excitation energy which could be explained by the decrease in conjugation of the phenyl π orbitals.

The enthalpy of another rotomer (assuming it exists) may be estimated from the relative intensities of the two sets of bands if we assume a model for the extent of equilibration of the rotomers during the course of cooling in the jet expansion. We have calculated the vibrational temperature T_{vib} under various expansion conditions (Fig. 14) for the 20 cm^{-1} ground state mode by fitting the relative intensities of the 0_0^0 and the -20 cm^{-1} hot band to a Boltzmann distribution. By assuming that thermodynamic cooling occurs (i.e., the distribution of rotomers reaches equilibrium at T_{vib}), then the relative intensities of the 0_0^0 for both rotomers may be used to estimate ΔH by fitting to a Boltzmann distribution at T_{vib}. Values of ΔH calculated in this way range from 11 to 15 cm^{-1}.

We should mention that there are some puzzling features that are not explained by the above picture. The assignment of the 26 cm^{-1} band is unclear although it has the spectral characteristics [Fig. 16(a)] of the second rotomer. It is also unclear whether the 26–39 cm^{-1} and the 83–95 cm^{-1} frequency differences are related or coincidental. Only the 39 cm^{-1} band, however, forms combinations with the 83 and 95 cm^{-1} bands. Although the 122 cm^{-1} band could be due to either the 26 + 95 or the 39 + 83 cm^{-1} combination, the dispersed fluorescence spectrum in Fig. 16(c) supports the latter assignment. Finally, we note that a very weak band at 75 cm^{-1} appears in excitation under reduced cooling conditions and forms combinations with the 83 and 95 cm^{-1} bands. We cannot rule out the possibility that this band represents the overtone of the 39 cm^{-1} band. It is possible, for instance, that the low frequency bands are fundamentals whose potentials and therefore vibronic transition probabilities are strongly affected (i.e., distorted) by rotational energy.[32]

V. CONCLUSION

As part of an overall study of the dynamics of *t*-stilbene photoisomerization, a thorough vibrational analysis of S_0 and S_1 was carried out and reported in this paper. The highlights of this study can be summarized as follows:

TABLE VIII. Comparison of dispersed fluorescence spectra to examine the possibility of different rotomers of *t*-stilbene.

h_{12}			d_{12}		
I (0^0)	II (S_1 + 39)[a]		I (0^0)	II (S_1 + 36)[a]	
0(100)[b]	0(100)		0(100)	0(100)	
20(28)	23(78)		17(22)	20(79)	
44(8)	49(82)		40(8)	45(95)	
66(–)	67(11)			59(9)	
75(3)	82(7)		67(4)	70(6)	
119(12)	115(11)		105(14)	104(13)	
204(71)	199(58)	25_1^0[c]	191(70)	187(53)	25_1^0
			231(sh)[d]	236(32)	
	253(16)			251(42)	
	265(sh)				
264(4)[d]	272(21)				
404(13)	395(13)		382(8)		
413(28)	409(37)	25_2^0	388(38)	388(37)	25_2^0
612(14)	605(11)	25_3^0	576(9)	572(7)	25_3^0
624(11)	626(16)		592(14)	590(16)	

[a]Excitation band corresponding to assumed 0^0 of the less favored rotomer.
[b]Frequencies are reported in cm^{-1} relative to the 0_0^0. Values in parentheses are relative intensities.
[c]Assignment of the ν_{25} progression.
[d]The corresponding band in II for this mode is uncertain.

Downloaded 21 Dec 2005 to 131.215.225.171. Redistribution subject to AIP license or copyright, see http://jcp.aip.org/jcp/copyright.jsp

(i) The low frequency modes in S_0 and S_1 have been resolved and assigned. The frequencies of these modes are very different in the two electronic states which has been interpreted as a strong mixing of the S_0 vibrations in S_1. The assignments of ethylene and benzene-type modes have also been made.

(ii) The very low frequencies observed are indicative of a_u modes which are active for a *t*-stilbene molecule with propeller-like geometry (i.e., C_2 symmetry) due to out-of-plane rotation of the phenyl groups.

(iii) The dispersed fluorescence spectrum from the 25^1 level reveals a novel interference effect whereby the 25_1^1 transition is completely absent. By combining a Franck–Condon analysis of the ν_{25} with a normal mode calculation, the change in the C_e–C_e–φ bond angle upon electronic transition was determined to be $1.3 \pm 0.3°$. The amplitude of this bend coordinate for the symmetric ν_{25} bend mode is $|\langle \Delta\varphi \rangle^2|^{1/2} = 1.0 \pm 0.2°$. The change in geometry is attributed to a delocalization of C_e–C_e double bond character to the C_e–φ bond.

(iv) Many observed spectral features are relevant to isomerization. The dispersed fluorescence spectra exhibit a pronounced broadening with excess S_1 vibrational energy and become totally diffuse at $\geqslant 1200\ \text{cm}^{-1}$. This corresponds approximately to the barrier height to reaction of 1100–1200 cm^{-1}. The fluorescence excitation spectra display a rapid decrease in intensity at higher energies due to isomerization which competes with radiative decay. The change in the C_e–C_e–φ bond angle determined from the Franck–Condon and normal mode analysis is consistent with the initial step towards isomerization since a decrease in this bend angle is expected as the π bonding in the C_e–C_e bond becomes delocalized into the C_e–φ bond.

ACKNOWLEDGMENTS

We gratefully acknowledge the National Science Foundation for support of this work under Grant No. CHE-8211356. We are particularly indebted to Professor A. Warshel for providing us with the normal mode analysis of *t*-stilbene and the figure of the ν_{25} normal coordinate. We also wish to thank Professor D. A. Evans and Mr. Robert Dow for assistance in recording the gas chromatographs of *t*-stilbene.

[1](a) A. H. Zewail, Faraday Discuss. Chem. Soc. **75**, 315 (1983); (b) A. H. Zewail, Laser Chem. **2**, 55 (1983); (c) P. M. Felker and A. H. Zewail, in *Applications of Picosecond Spectroscopy to Chemistry*, edited by K. B. Eisenthal (D. Reidel, Holland, 1984), p. 273.
[2]W. R. Lambert, P. M. Felker, and A. H. Zewail, J. Chem. Phys. **81**, 2209, 2217 (1984).
[3]J. A. Syage, P. M. Felker, and A. H. Zewail, J. Chem. Phys. **81**, 2233 (1984).
[4]J. A. Syage, F. Al Adel, and A. H. Zewail, Chem. Phys. Lett. **103**, 15 (1983).
[5]J. F. Shepanski, B. W. Keelan, and A. H. Zewail, Chem. Phys. Lett. **103**, 9 (1983).
[6]J. A. Syage, W. R. Lambert, P. M. Felker, A. H. Zewail, and R. M. Hochstrasser, Chem. Phys. Lett. **88**, 268 (1982).
[7](a) J. W. Perry, N. F. Scherer, and A. H. Zewail, Chem. Phys. Lett. **103**, 1 (1983); (b) N. F. Scherer, J. F. Shepanski, and A. H. Zewail, J. Chem. Phys. **81**, 2181 (1984).
[8]J. A. Syage, P. M. Felker, and A. H. Zewail, J. Chem. Phys. **81**, 2217 (1984).
[9]J. Saltiel, J. D'Agostino, E. D. Megarity, L. Metts, K. R. Neuberger, M. Wrighton, and O. C. Zafiriou, Org. Photochem. **3**, 1 (1973).
[10]G. Rothenberger, D. K. Negus, and R. M. Hochstrasser, J. Chem. Phys. **79**, 5360 (1983).
[11](a) M. Sumitani, N. Nakashima, and K. Yoshihara, Chem. Phys. Lett. **68**, 255 (1979); (b) F. Heisel, J. A. Miehe, and B. Sipp, *ibid.* **61**, 115 (1979).
[12](a) B. I. Greene, R. M. Hochstrasser, and R. B. Weisman, J. Chem. Phys. **71**, 544 (1979); (b) Chem. Phys. **48**, 289 (1980).
[13]A. Amirav and J. Jortner, Chem. Phys. Lett. **95**, 295 (1983).
[14]T. S. Zwier, E. Carrasquillo M., and D. H. Levy, J. Chem. Phys. **78**, 5493 (1983).
[15]R. H. Dyke and D. S. McClure, J. Chem. Phys. **36**, 2326 (1962).
[16]Z. Meić and H. Güsten, Spectrochim. Acta Part A **34**, 101 (1978).
[17](a) A. Bree and M. Edelson, Chem. Phys. **51**, 77 (1980); (b) M. Edelson and A. Bree, Chem. Phys. Lett. **41**, 562 (1976).
[18]A. Bree, R. Zwarich, and M. Edelson, Spectrochim. Acta Part A **38**, 719 (1982).
[19]W. M. Hetherington III and B. S. Hudson, Chem. Phys. Lett. **65**, 261 (1979).
[20]G. Hohlneicher and B. Dick, J. Photochem. (submitted).
[21]B. M. Pierce and R. R. Birge, J. Phys. Chem. **86**, 2651 (1982).
[22]A. Warshel, J. Chem. Phys. **62**, 214 (1975).
[23]C. Pecile and B. Lunelli, Can. J. Chem. **47**, 243 (1969).
[24]G. Varsanyi, *Assignments for Vibrational Spectra of Seven Hundred Benzene Derivatives* (Wiley, New York, 1974).
[25]J. B. Hopkins, D. E. Powers, and R. E. Powers, J. Chem. Phys. **72**, 5039 (1980).
[26](a) T. R. Gilson, J. M. Hollas, E. Khalilipour, and J. V. Warrington, J. Mol. Spectrosc. **73**, 234 (1978); (b) J. M. Hollas, E. Khalilipour, and S. N. Thakur, *ibid.* **73**, 240 (1978); (c) D. A. Condirston and J. D. Laposa, *ibid.* **63**, 466 (1976).
[27](a) J. M. Hollas and T. Ridley, J. Mol. Spectrosc. **89**, 232 (1981); (b) J. M. Hollas, H. Musa, T. Ridley, P. H. Turner, and K. H. Weisenberger, *ibid.* **94**, 437 (1982).
[28]W. R. Lambert, P. M. Felker, J. A. Syage, and A. H. Zewail, J. Chem. Phys. **81**, 2195 (1984).
[29](a) T. L. Gustafson, D. M. Roberts, and D. A. Chernoff, J. Chem. Phys. **79**, 1559 (1983); (b) H. Hamaguchi, T. Urano, and M. Tasumi, Chem. Phys. Lett. **106**, 153 (1984).
[30]J. B. Coon, R. E. DeWames, and C. M. Loyd, J. Mol. Spectrosc. **8**, 285 (1962).
[31]F. Ansbacher, Z. Naturforsch Teil A **14**, 889 (1959).
[32]A. Warshel (personal communication and unpublished results).
[33]A. Warshel, Isr. J. Chem. **11**, 709 (1973).
[34]R. M. Hochstrasser, G. W. Scott, and A. H. Zewail, Mol. Phys. **36**, 475 (1978).
[35](a) G. Orlandi and W. Siebrand, Chem. Phys. Lett. **30**, 352 (1973); (b) G. Orlandi, P. Palmiari, and G. Poggi, J. Am. Chem. Soc. **101**, 3492 (1979); (c) F. Momicchioli, M. C. Bruni, I. Baraldi, and G. R. Corradini, J. Chem. Soc. Faraday Trans. 2, **70**, 1325 (1974); (d) G. Olbrich, Ber. Bunsenges. Phys. Chem. **86**, 209 (1982); (e) P. Tavan and K. Schulten, Chem. Phys. Lett. **56**, 200 (1978); (f) D. L. Beveridge and H. H. Jaffé, J. Am. Chem. Soc. **87**, 5340 (1965).
[36](a) C. J. Finder, M. G. Newton, and N. L. Allinger, Acta Crystallogr. Sect. B **30**, 411 (1974); (b) A. Hoekstra, P. Meertens, and A. Vos, *ibid.* **31**, 2813 (1975); (c) J. Bernstein, *ibid.* **31**, 1268 (1975).
[37]M. Traetteberg, E. B. Frantsen, F. C. Mijlhoff, and A. Hoekstra, J. Mol. Struct. **26**, 57 (1975).
[38]T. Kobayashi, H. Suzuki, and K. Ogawa, Bull. Chem. Soc. Jpn. **55**, 1734 (1982).
[39]F. E. Doany, B. I. Greene, and R. M. Hochstrasser, Chem. Phys. Lett. **75**, 206 (1980).

Downloaded 21 Dec 2005 to 131.215.225.171. Redistribution subject to AIP license or copyright, see http://jcp.aip.org/jcp/copyright.jsp